

$B \rightarrow K\ell^+\ell^-$ decay at large hadronic recoil

A. Khodjamirian, Th. Mannel and Y.-M. Wang*

*Theoretische Physik 1, Naturwissenschaftlich-Technische Fakultät, Universität Siegen,
D-57068 Siegen, Germany*

ABSTRACT: We predict the amplitude of the $B \rightarrow K\ell^+\ell^-$ decay in the region of the dilepton invariant mass squared $0 < q^2 \leq m_{J/\psi}^2$, that is, at large hadronic recoil. The $B \rightarrow K$ form factors entering the factorizable part of the decay amplitude are obtained from QCD light-cone sum rules. The nonlocal effects, generated by the four-quark and penguin operators combined with the electromagnetic interaction, are calculated at $q^2 < 0$, far below the hadronic thresholds. For hard-gluon contributions we employ the QCD factorization approach. The soft-gluon nonfactorizable contributions are estimated from QCD light-cone sum rules. The result of the calculation is matched to the hadronic dispersion relation in the variable q^2 , which is then continued to the kinematical region of the decay. The overall effect of nonlocal contributions in $B \rightarrow K\ell^+\ell^-$ at large hadronic recoil is moderate. The main uncertainty of the predicted $B \rightarrow K\ell^+\ell^-$ partial width is caused by the $B \rightarrow K$ form factors. Furthermore, the isospin asymmetry in this decay is expected to be very small. We investigate the deviation of the observables from the Standard Model predictions by introducing a generic new physics contribution to the effective Hamiltonian.

KEYWORDS: B-Physics, Rare Decays, QCD, Sum rules.

*Address after September 30, 2012: Physik Department T31, James-Franck-Straße, Technische Universität München, D-85748 Garching, Germany.

Contents

1. Introduction	1
2. Hadronic effects in the decay amplitude	3
3. Hadronic matrix elements in the spacelike region	7
3.1 Factorizable loop	7
3.2 Factorizable NLO contributions	8
3.3 Nonfactorizable soft-gluon contributions	9
3.4 Nonfactorizable spectator contributions	10
3.5 Weak annihilation	11
3.6 Power counting	11
4. Soft-gluon contribution of the O_{8g} operator	12
5. Nonlocal hadronic effects in timelike region	15
6. Numerical results	19
7. Observables in $B \rightarrow K\ell^+\ell^-$	23
8. Discussion	26

1. Introduction

After a very successful start, the LHCb experiment has already provided new measurements of exclusive flavour-changing neutral current (FCNC) decays of B mesons [1]-[4], continuing the studies of these decays carried out at B -factories [5, 6] and Tevatron [7]. The favourite decay channel is $B \rightarrow K^*\ell^+\ell^-$ where a rich kinematics allows one to measure several nontrivial observables sensitive to the underlying FCNC $b \rightarrow s\ell^+\ell^-$ transitions. So far, the measurements of these decays did not reveal any significant deviation from Standard Model (SM). In particular, the zero crossing point of the forward-backward asymmetry in $B \rightarrow K^*\ell^+\ell^-$ predicted in SM has recently been observed [1] within the expected interval of the variable q^2 , the invariant mass squared of the lepton pair. Meanwhile, the measured isospin asymmetry in $B \rightarrow K^{(*)}\ell^+\ell^-$, allows for the values larger than expected in SM, hence, this observable deserves a further careful study.

The theory of rare semileptonic decays, such as $B \rightarrow K^{(*)}\ell^+\ell^-$, suffers from hadronic uncertainties. Apart from the heavy-to-light form factors, determining the contributions of the leading FCNC operators in the effective Hamiltonian, the decay amplitudes receive

contributions of the current-current and penguin operators combined with the lepton-pair emission via electromagnetic (e.m.) interaction. A common feature of all these effects is that they are *nonlocal* because the quark-flavour transition is separated from the virtual-photon emission, and the characteristic distances of this separation are not necessarily small. The most important nonlocal contribution is generated by the current-current operators with c quarks, forming “charm-loops” after photon emission. The charm loops turn into intermediate charmonium states at $q^2 \geq m_{J/\psi}^2$. The nonlocal effects in $B \rightarrow K^{(*)}\ell^+\ell^-$ have been estimated in the literature, within different models and approximations. The most complete analysis at large hadronic recoil (low q^2) was done in the QCD-factorization framework in [8]. In that approach, the quark-gluon diagrams of various factorizable and nonfactorizable nonlocal contributions were calculated at timelike q^2 , below charmonium thresholds.

In our previous paper [9] the soft-gluon emission from the charm loop in $B \rightarrow K^{(*)}\ell^+\ell^-$ – an effect not accessible in QCD factorization approach – was estimated. To that end, the light-cone operator product expansion (OPE) at $q^2 \ll 4m_c^2$ was employed and the soft-gluon emission was effectively resummed in a nonlocal quark-antiquark-gluon operator. The resulting hadronic matrix elements were then estimated using QCD light-cone sum rules (LCSR), i.e., the same approach which is used to calculate the $B \rightarrow K^{(*)}$ form factors. Being suppressed by the powers of $\Lambda_{QCD}^2/(4m_c^2 - q^2)$, the soft-gluon contribution to the decay amplitude grows at q^2 approaching the $\bar{c}c$ threshold, To avoid the divergence at $q^2 \simeq 4m_c^2$, the hadronic dispersion relation in the q^2 channel was employed in [9] and matched to the calculation result at $q^2 \ll 4m_c^2$.

The aim of this paper is to perform a complete account of hadronic nonlocal effects for one particular channel $B \rightarrow K\ell^+\ell^-$. We will apply the same approach as in [9], this time including the complete effective Hamiltonian. In this case, light-quark loops also contribute to the amplitude, therefore we calculate the nonlocal effects in QCD in the spacelike region $q^2 < 0$, sufficiently far from all quark-antiquark thresholds. Soft-gluon emission evaluated in [9] is taken into account for quark loops with different flavours. In addition, we calculate a new effect of soft-gluon emission from the gluon-penguin operator applying the LCSR approach. We also take into account the hard-gluon NLO contributions. In the correlation functions used to derive LCSR’s, the hard-gluon exchanges generate multiloop and multiscale diagrams which demand dedicated calculational efforts that are far beyond our scope. Instead, we approximate the hard-gluon nonlocal effects, employing the QCD factorization approach [8] at $q^2 < 0$. Following [9], the physical region in $B \rightarrow K\ell^+\ell^-$ is accessed via hadronic dispersion relations in the variable q^2 . In these relations, in addition to the charmonium states, the light vector mesons contribute. Finally, we predict the observables for $B \rightarrow K\ell^+\ell^-$ including the differential width and isospin asymmetry. Our results are applicable at $q^2 \leq m_{J/\psi}^2$ where they are compared with the available experimental data.

The $B \rightarrow K\ell^+\ell^-$ decay channel chosen here has less observables and a smaller branching fraction than $B \rightarrow K^*\ell^+\ell^-$. In turn, the relative simplicity makes the kaon mode a more convenient study object for hadronic effects. First of all, the current accuracy of the $B \rightarrow K$ form factors is better than for $B \rightarrow K^*$ form factors. Note that the latter form

factors are available only in the quenched approximation of the lattice QCD. The $B \rightarrow K$ form factors used here are calculated from LCSR with kaon distribution amplitudes (DA's). These sum rules are free from the “systematic” uncertainty of LCSR's for $B \rightarrow K^*$ form factors caused by neglecting the $K^* \rightarrow K\pi$ width. The alternative LCSR's with B -meson DA's implicitly overcome this problem if one relies on the duality approximation in the K^* channel. However, the B -meson DA's still suffers from large uncertainties of their parameters, such as the inverse moment. Since the form factors not only determine the leading operator contributions but also enter the factorizable nonlocal effects, we expect that the hadronic input in $B \rightarrow K\ell^+\ell^-$ is currently under a better control than in $B \rightarrow K^*\ell^+\ell^-$. This circumstance strengthens the case for using the kaon channel as a perspective tool to trace generic new physics (see e.g., [10, 11]).

The plan of the paper is as follows. In Section 2 we define the nonlocal hadronic matrix elements entering the $B \rightarrow K\ell^+\ell^-$ amplitude. The nonlocal effects are listed in terms of quark-gluon diagrams. In Section 3 we present the corresponding hadronic matrix elements in the spacelike region obtained by combining LCSR's with the QCD factorization approach. In Section 4 the LCSR for the soft contribution of the gluon-penguin operator is derived. Furthermore, in Section 5 we specify the use of hadronic dispersion relations to access the physical region. In Section 6 the relevant numerical analysis is performed. The resulting predictions for the $B \rightarrow K\ell^+\ell^-$ differential width and isospin asymmetry are presented in Section 7 where we also discuss the influence of generic new physics on these observables. Section 8 is reserved for the concluding discussion and outlook. In Appendix A, the operators of the effective Hamiltonian and their Wilson coefficients are specified, Appendix B contains the definitions of B -meson DA's and Appendix C the expressions related to the LCSR derivation.

2. Hadronic effects in the decay amplitude

The $B \rightarrow K\ell^+\ell^-$ decay amplitude in SM is given by the matrix element of the $b \rightarrow s\ell^+\ell^-$ effective Hamiltonian [12, 13]:

$$H_{eff} = -\frac{4G_F}{\sqrt{2}}V_{tb}V_{ts}^* \sum_{i=1}^{10} C_i(\mu)O_i(\mu). \quad (2.1)$$

The effective local operators O_i and the numerical values of their Wilson coefficients C_i are presented in App. A. In this paper we generally neglect the CKM-suppressed contributions proportional to $V_{ub}V_{us}^*$, retaining them only in the calculation of the isospin asymmetry where their numerical impact is non-negligible.

In the decay amplitude we separate the dominant factorizable contributions of the

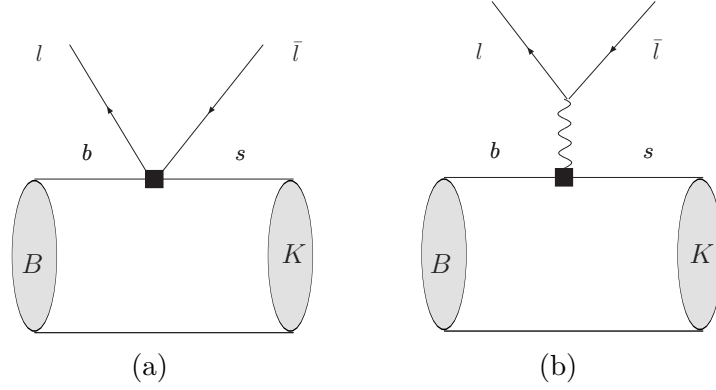


Figure 1: FCNC contributions to $B \rightarrow K \ell^+ \ell^-$ due to the effective operators $O_{9,10}$ (a) and O_7 (b) denoted as black squares.

operators $O_{7,9,10}$ (Fig. 1):

$$\begin{aligned}
A(B \rightarrow K \ell^+ \ell^-) &= -\langle K(p) \ell^+ \ell^- | H_{eff} | B(p+q) \rangle \\
&= \frac{G_F}{\sqrt{2}} \frac{\alpha_{em}}{\pi} V_{tb} V_{ts}^* \left[\bar{\ell} \gamma_\mu \ell p^\mu \left(C_9 f_{BK}^+(q^2) + \frac{2(m_b + m_s)}{m_B + m_K} C_7^{eff} f_{BK}^T(q^2) \right) \right. \\
&\quad \left. + \bar{\ell} \gamma_\mu \gamma_5 \ell p^\mu C_{10} f_{BK}^+(q^2) - (16\pi^2) \frac{\bar{\ell} \gamma_\mu \ell}{q^2} \mathcal{H}_\mu^{(BK)} \right], \quad (2.2)
\end{aligned}$$

where $f_{BK}^{+(T)}(q^2)$ is the usual $B \rightarrow K$ vector (tensor) form factor and, according to [13], $C_7^{eff} = C_7 - \frac{1}{3}C_5 - C_6$. The nonlocal hadronic matrix element

$$\begin{aligned}
\mathcal{H}_\mu^{(BK)} &= i \int d^4x e^{iq \cdot x} \langle K(p) | T \left\{ j_\mu^{em}(x), \left[C_1 O_1^{(c)}(0) + C_2 O_2^{(c)}(0) \right. \right. \\
&\quad \left. \left. + \sum_{k=3-6,8g} C_k O_k(0) \right] \right\} | B(p+q) \rangle = [(p \cdot q) q^\mu - q^2 p^\mu] \mathcal{H}^{(BK)}(q^2) \quad (2.3)
\end{aligned}$$

contains the contributions of all remaining operators in (2.1) combined with the quark electromagnetic (e.m.) current $j_\mu^{em} = \sum_{q=u,d,s,c,b} Q_q \bar{q} \gamma_\mu q$. Our definition of $\mathcal{H}^{(BK)}$ differs from the one used in [9] by including the quark-charge factors Q_q . Furthermore, due to renormalization effects, one has to replace [13] above $C_{8g} \rightarrow C_8^{eff} = C_{8g} + (4C_3 - C_5)/3$. After substituting (2.3) in (2.2), due to conservation of the leptonic current, only the structure $q^2 p^\mu$ remains in (2.3), canceling the photon propagator $1/q^2$. Hence, opposite to the case of $B \rightarrow K^* \ell^+ \ell^-$, there is no kinematic enhancement of the $B \rightarrow K \ell^+ \ell^-$ amplitude at low q^2 . Dividing the invariant amplitude $\mathcal{H}^{(BK)}(q^2)$ by the form factor $f_{BK}^+(q^2)$, it is convenient to represent the nonlocal hadronic effect in a form of a (process- and q^2 -dependent) correction to the coefficient C_9 ,

$$\Delta C_9^{(BK)}(q^2) = \frac{16\pi^2 \mathcal{H}^{(BK)}(q^2)}{f_{BK}^+(q^2)}. \quad (2.4)$$

The contributions to the nonlocal amplitude (2.3) are usually represented in a form of quark-gluon diagrams shown one by one in Figs. 2 - 5. The dominant contribution

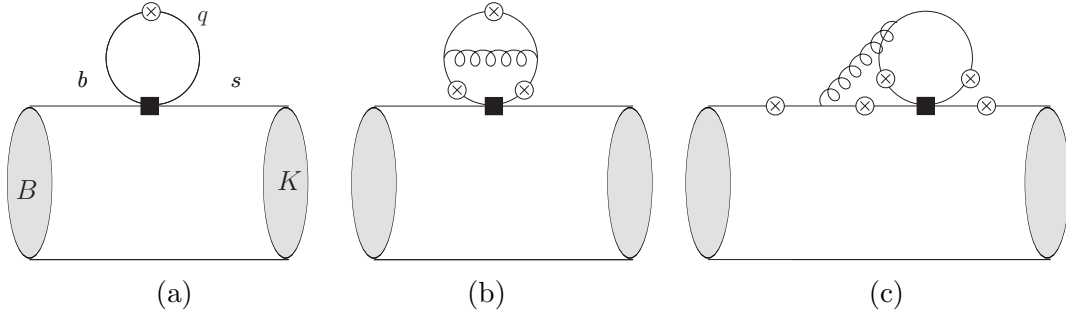


Figure 2: Factorizable quark-loop contributions to $B \rightarrow K\ell^+\ell^-$ due to four-quark effective operators $O_{1,2}^c$ and O_{3-6} . Crossed circles denote the possible points of the virtual photon emission. Diagrams similar to (c) with the gluon line attached to the s -quark line are not shown.

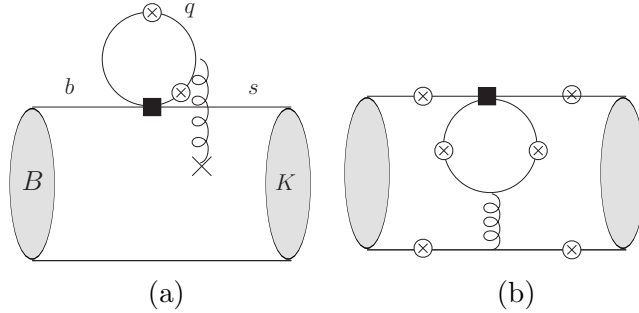


Figure 3: Nonfactorizable quark-loop contributions to $B \rightarrow K\ell^+\ell^-$: (a) with soft gluon (denoted by crossed line) and (b) with hard-gluon.

is generated by the operators $O_{1,2}^{(c)}$ with large Wilson coefficients and corresponds to the diagrams shown in Figs. 2, 3, where $q = c$ (the “charm-loop” effect). This contribution includes intermediate vector charmonium states in the upper part of the decay kinematical region, $m_{J/\psi}^2 < q^2 < (m_B - m_K)^2$. Measuring $B \rightarrow K\ell^+\ell^-$ in the vicinity of $q^2 = m_\psi^2$ ($\psi = J/\psi, \psi(2S), \dots$), one practically observes a combination of the weak nonleptonic ($B \rightarrow \psi K$) and leptonic ($\psi \rightarrow \ell^+\ell^-$) decays, whereas the genuine FCNC process $b \rightarrow s\ell^+\ell^-$, driven by the effective operators $O_{7,9,10}$, turns into a tiny background. Note that the interval $4m_D^2 < q^2 < (m_B - m_K)^2$ also contains broad charmonium resonances. To avoid the charmonium background, all experimental measurements of $B \rightarrow K\ell^+\ell^-$ implement a subtraction of the two q^2 -bins around $m_{J/\psi}^2$ and $m_{\psi(2S)}^2$.

In this paper we concentrate on the region of small and intermediate lepton-pair masses, $q^2 < m_{J/\psi}^2$. In this region the charm-loop effect is present in the form of a virtual $\bar{c}c$ fluctuation. The latter is usually approximated by c -quark loop diagrams, starting from the leading-order (LO) simple loop in Fig. 2(a) and including the gluon corrections. A characteristic feature of this perturbative approximation at timelike q^2 is a “kink” in the predicted differential width, due to the onset of the imaginary part of the c -quark loop at the threshold $q^2 = 4m_c^2 < m_{J/\psi}^2$. To avoid this unphysical effect, in what follows we employ the hadronic dispersion relation in the q^2 variable, following [9]. In this paper we

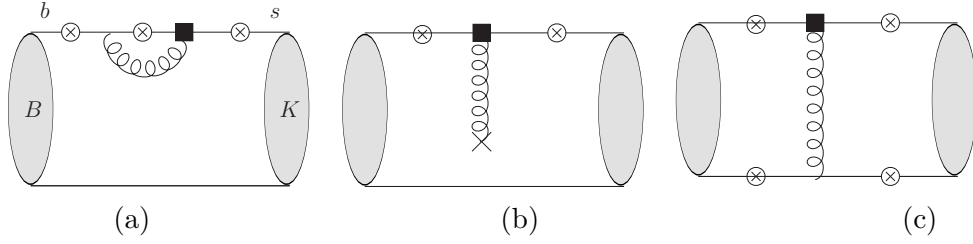


Figure 4: Contributions of the O_{sg} operator to $B \rightarrow K\ell^+\ell^-$: (a) factorizable, (b) and (c) nonfactorizable with soft and hard gluon, respectively.

also include the contributions to $\mathcal{H}^{(BK)}(q^2)$ stemming from the operators with light quarks. Hence, to stay away from quark-antiquark thresholds, all quark-gluon diagrams shown in Figs. 2-5 have to be calculated at $q^2 < 0$ with sufficiently large $|q^2|$.

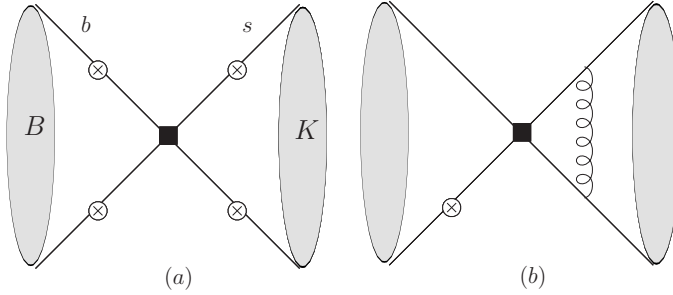


Figure 5: Weak annihilation contribution to $B \rightarrow K\ell^+\ell^-$ amplitude: (a) in LO and (b) one of the NLO hard-gluon exchange diagrams.

Before considering separate contributions to the hadronic matrix element $\mathcal{H}^{(BK)}(q^2)$, the following comment is in order. A close inspection of the quark-loop diagrams at NLO shows that also at $q^2 < 0$, below all hadronic thresholds in the e.m. current channel, the diagrams develop an imaginary part. This is a clear signal that the intermediate hadronic states in the amplitude $\mathcal{H}^{(BK)}(q^2 < 0)$ go on shell, so that the quark-gluon diagrams provide only a local duality approximation for this amplitude. For example, let us consider a diagram similar to the one shown in Fig. 2(c), but with the photon emitted from the s -quark. This diagram and one of its hadronic counterparts are shown in Fig. 6. To describe this hadronic transition in more detail we choose $q = c, q' = d$ for definiteness. In this case \bar{B}^0 -meson decays to an on-shell hadronic state with the quark content $(\bar{c}s)(cd)$ (e.g., $\bar{B}^0 \rightarrow D_s^- D^+$) which then converts via strong and e.m. interaction into the final \bar{K}^0 meson and a lepton pair ($D_s^- D^+ \rightarrow \bar{K}^0 \ell^+ \ell^-$). This hadronic mechanism involving multiple intermediate states with the same quantum numbers contributes to the strong final-state interaction in $B \rightarrow K\ell^+\ell^-$. Approximating the sum over intermediate hadronic states with a quark-level diagram is justified by the large mass of the initial B -state and the large recoil of the final hadron. This approximation is similar to the one used in the QCD factorization approach to exclusive nonleptonic B -decays [14].

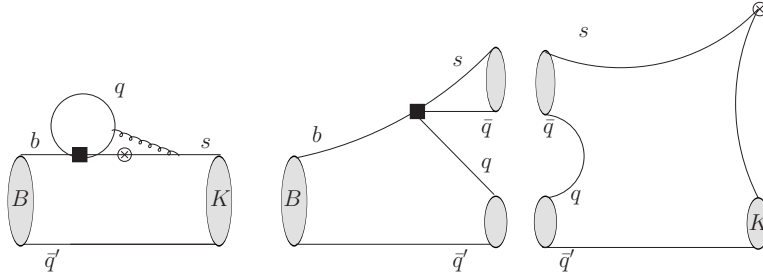


Figure 6: The NLO quark-loop diagram of $B \rightarrow K \ell \ell$ decay (left) and one of its hadronic counterparts (right) containing the intermediate pair of on-shell hadrons with flavour content $(s\bar{q})(q\bar{q}')$.

Let us emphasize another important point. The imaginary part of the amplitude $\mathcal{H}^{(BK)}(q^2)$ at spacelike q^2 is generated by the discontinuities in the variable $(p+q)^2$. In $B \rightarrow K \ell^+ \ell^-$ with an on-shell initial B meson, this variable is fixed at $(p+q)^2 = m_B^2$. To illustrate a generic two-variable kinematics, one has to consider a correlation function where, instead of the B -meson state in (2.3), a vacuum state is taken and a quark current $\bar{q}' \gamma_5 b$ with $B_{q'}$ -meson quantum numbers is added to the time-ordered operator product, with the momentum squared $(p+q)^2$. The variable q^2 is kept fixed and spacelike. Still, the correlation function has discontinuities in the variable $(p+q)^2$ located below the B -meson pole and generated by intermediate $(s\bar{q})(q\bar{q}')$ states. Note that the presence of these “parasitic” intermediate states in the B -meson channel of the correlation function is caused by the absence of external 4-momentum in the effective operator vertex in (2.3). Returning to the calculation of the hadronic amplitude $\mathcal{H}^{(BK)}(q^2)$, we conclude that using OPE near the light-cone, $x^2 \sim 0$ in (2.3) and restricting the calculation to $q^2 < 0$, one cannot avoid using quark-gluon diagrams at a timelike (albeit large) value of the second kinematical variable $(p+q)^2$. Hence, strictly speaking, the calculation procedure used here relies not entirely on OPE but also on the local quark-hadron duality.

3. Hadronic matrix elements in the spacelike region

In this section we present separate contributions to the hadronic amplitude $\mathcal{H}_{BK}(q^2 < 0)$ defined in (2.3), including all effective operators entering H_{eff} and taking into account different possible quark topologies.

3.1 Factorizable loop

In LO, the contribution of the four-quark operators to $B \rightarrow K \ell^+ \ell^-$ is shown in Fig. 2(a). In addition to the dominant c -quark loop from the current-current operators $O_{1,2}^{(c)}$ it also contains quark loops with various flavours, originating from the quark-penguin operators O_{3-6} . In the adopted convention for the effective operators the sum over all LO loops can

be written as

$$\begin{aligned}
\mathcal{H}_{fact,LO}^{(BK)}(q^2) &= \frac{1}{8\pi^2} \left\{ Q_c \left(\frac{C_1}{3} + C_2 \right) g(m_c^2, q^2) \right. \\
&\quad \left. + \left(\frac{C_3}{3} + C_4 \right) \left[Q_s g(m_s^2, q^2) + Q_b g(m_b^2, q^2) \right] \right. \\
&\quad \left. + \left(C_3 + \frac{C_4}{3} + C_5 + \frac{C_6}{3} \right) \sum_{q=u,d,s,c,b} Q_q \bar{g}(m_q^2, q^2) \right\} f_{BK}^+(q^2), \tag{3.1}
\end{aligned}$$

where

$$g(m_q^2, q^2) = - \left(\ln \frac{m_q^2}{\mu^2} + 1 \right) + q^2 \int_{4m_q^2}^{+\infty} ds \frac{\sqrt{1 - \frac{4m_q^2}{s}} \left(1 + \frac{2m_q^2}{s} \right)}{s(s - q^2)}, \tag{3.2}$$

is the well-known loop function, μ is the renormalization scale and $\bar{g}(m_q^2, q^2) = g(m_q^2, q^2) + 1$. The definition of $g(m_q^2, q^2)$ used in [9] differs from the above by the factor 4/9. Since here we employ the loop diagrams at $q^2 < 0$, that is below all quark-antiquark thresholds, only the real part of $g(m_q^2, q^2)$ is needed. Hereafter we also neglect the mass of the u and d quarks, so that for them the loop function is $g(0, q^2) = 2/3 - \ln(-q^2/\mu^2)$.

3.2 Factorizable NLO contributions

The NLO corrections to the quark loops include the diagrams shown in Figs. 2(b,c). In the same order of perturbative expansion the gluon-penguin operator enters with the diagrams in Fig. 4(a). The characteristic feature of all these diagrams [8]¹ is that the corresponding hadronic matrix elements are *factorizable* in the same form as the LO contributions considered in the previous section. Following [8], we extract the hard-scattering coefficient functions multiplying the $B \rightarrow K$ form factor from the NLO diagrams for the $b \rightarrow s\ell^+\ell^-$ decay rates calculated in [16, 17].

Summing over all contributing operators, the factorizable NLO contributions to the hadronic amplitude can be written as

$$\begin{aligned}
\mathcal{H}_{fact,NLO}^{(BK)}(q^2) &= -\frac{\alpha_s}{32\pi^2} \frac{m_b}{m_B} \left\{ C_1 F_2^{(7)}(q^2) + C_8^{eff} F_8^{(7)}(q^2) \right. \\
&\quad \left. + \frac{m_B}{2m_b} \left[C_1 F_2^{(9)}(q^2) + 2C_2 \left(F_1^{(9)}(q^2) + \frac{1}{6} F_2^{(9)}(q^2) \right) + C_8^{eff} F_8^{(9)}(q^2) \right] \right\} f_{BK}^+(q^2). \tag{3.3}
\end{aligned}$$

The definitions and nomenclature of the indices of the functions $F_{1,2,8}^{(7,9)}$ are the same as in [16, 17], where $F_{1,2}^{(7,9)}$ are expressed as a double expansion in $\hat{s} = q^2/m_b^2$ and $\hat{m}_c^2 = m_c^2/m_b^2$. It has been shown in [16, 17] that keeping the terms up to the third power of \hat{s} and \hat{m}_c^2 provides a sufficient numerical accuracy in the region $0.05 \leq \hat{s} \leq 0.25$. Here we use these expansions at $q^2 < 0$, restricting ourselves to $|\hat{s}| < 0.25$. For $F_8^{(7,9)}$ we use the expressions derived in [8]. Note that the NLO diagrams generate an imaginary part in the coefficient

¹For an earlier estimate of this effect within quark model see, e.g. [15].

functions entering (3.3), which, as discussed in the previous section, has to be interpreted as a quark-hadron duality counterpart of the strong rescattering in the hadronic amplitude.

A dedicated LCSR calculation of the hadronic matrix element (3.3) at $q^2 < 0$ is also possible. One has to introduce a correlation function where the B meson is represented with its DA's and K meson is interpolated with a quark current. However, in the case of four-quark operators, the complexity of the two-loop diagrams with several momentum/mass scales emerging in the OPE for the correlation function makes the computation of hard-gluon contributions from LCSR's a very difficult task. On the other hand, the diagrams for the correlation function with the gluon-penguin operator have only one loop and can in principle be calculated in future, to be compared with the QCD factorization results which are used here.

3.3 Nonfactorizable soft-gluon contributions

The contributions to the hadronic amplitude $\mathcal{H}_{BK}(q^2)$ that are beyond QCD factorization, include also the soft-gluon emission from the quark loop, as shown in Fig. 3(a). In [9] the dominant part of this effect, caused by the c -quark loop was estimated using the light-cone OPE at $q^2 \ll 4m_c^2$, where this power correction is suppressed by the inverse power of $(4m_c^2 - q^2)$ with respect to the LO loop. Here we also include the contributions of the soft-gluon emission from the quark loops generated by the quark-penguin operators. In presence of the light-quark loops, we shift the calculation to $q^2 < 0$, so that $|q^2| \gg \Lambda_{QCD}^2$.

The $B \rightarrow K$ hadronic matrix element for the soft-gluon emission from the loop with a generic quark flavour q can be easily derived from the results of [9]. At $q^2 \ll 4m_q^2$, the soft-gluon emission effect is reduced to a hadronic matrix element

$$\langle \bar{K}(p) | \tilde{\mathcal{O}}_\mu(m_q, q) | B(p+q) \rangle = [(p \cdot q)q_\mu - q^2 p_\mu] \tilde{\mathcal{A}}(m_q^2, q^2), \quad (3.4)$$

where the operator $\tilde{\mathcal{O}}_\mu(m_q, q)$ is equal to the nonlocal effective operator $\tilde{\mathcal{O}}_\mu(q)$ defined in (3.14) of [9] with the replacement $m_c \rightarrow m_q$ in the coefficient function $I_{\mu\rho\alpha\beta}(q, \omega)$ given in (3.15). Collecting the contributions from all four-quark operators, we obtain for the soft-gluon emission effect

$$\begin{aligned} \mathcal{H}_{soft,4q}^{(BK)}(q^2) = & 2\{Q_c(C_1 + C_4 - C_6)\tilde{\mathcal{A}}(m_c^2, q^2) + (C_4 - C_6)(Q_u + Q_d)\tilde{\mathcal{A}}(0, q^2) \\ & + (C_3 + C_4 - C_6)[Q_b\tilde{\mathcal{A}}(m_b^2, q^2) + Q_s\tilde{\mathcal{A}}(m_s^2, q^2)]\}. \end{aligned} \quad (3.5)$$

Note that in this contribution the dominant charm-loop part has an enhanced Wilson coefficient with respect to the one in the LO expression (3.1). At $q^2 < 0$ the hadronic matrix element $\tilde{\mathcal{A}}(m_q^2, q^2)$ is obtained from LCSR with B -meson DA's, using the analytic expression (4.8) in [9] derived for the c -quark case. The quark-flavour dependence is concentrated in the denominator which stems from the coefficient function of the effective operator.

Finally, there is also a soft-gluon emission generated by the O_{8g} operator as shown in Fig. 4b. It is a nonfactorizable effect, so far not taken into account. In the next section we will derive a dedicated LCSR for the corresponding hadronic matrix element.

Note that within the LCSR approach a systematic separation of ‘‘hard’’- and ‘‘soft’’-gluon contributions, with high and low average virtualities, respectively, is possible, attributing them to different terms in the OPE. E.g., in the sum rules with B -meson DA's the

soft-gluon contributions enter the terms with three-particle DA's, whereas the hard-gluon contributions enter the NLO coefficient functions in the terms containing quark-antiquark DA's. Here we use LCSR's to compute the soft-gluon contributions whereas the hard-gluon effects are approximated by QCD factorization.

3.4 Nonfactorizable spectator contributions

A highly-virtual (“hard”) gluon emitted from the intermediate quark loop or from the O_{8g} operator vertex, can be absorbed by the spectator quark in the $B \rightarrow K$ transition, generating an additional contribution – see Fig. 3(b) or Fig. 4(c), respectively – which cannot be reduced to the $B \rightarrow K$ form factors. In [8] a factorization formula for this contribution was derived in terms of the hard-scattering kernels convoluted with the B -meson and kaon DA's:

$$\mathcal{H}_{nonf,spect.}^{(BK)}(q^2) = \frac{\alpha_s C_F}{32\pi N_c} \frac{f_B f_K m_b}{m_B^2} \sum_{\pm} \int \frac{d\omega}{\omega} \phi_B^{\pm}(\omega) \int_0^1 du \varphi_K(u) T_{\pm}^{(1)}(u, \omega), \quad (3.6)$$

where the standard definition (see e.g., [18]) of two-particle B meson DA's $\phi_B^{\pm}(\omega)$ and of the twist-2 DA of the kaon $\varphi_K(u)$ is used. The NLO hard kernels $T_{\pm}^{(1)}(u, \omega)$ corresponding to the sum of the diagrams in Fig. 3(b) and Fig. 4(c) are taken from [8]:

$$\begin{aligned} T_+^{(1)}(u, \omega) = & -\frac{m_B}{m_b} [Q_c t_{||}(u, m_c)(C_1 + C_4 - C_6) + Q_b t_{||}(u, m_b)(C_3 + C_4 - C_6) \\ & + Q_s t_{||}(u, m_s)(C_3 + C_4 - C_6) + Q_u t_{||}(u, 0)(C_4 - C_6) \\ & + Q_d t_{||}(u, 0)(C_4 - C_6)], \end{aligned} \quad (3.7)$$

$$\begin{aligned} T_-^{(1)}(u, \omega) = & -Q_q \frac{m_B \omega}{m_B \omega - q^2} \left\{ \frac{8m_B}{3m_b} [g(m_c^2, \bar{u}m_B^2 + uq^2)(C_1 + C_4 + C_6) \right. \\ & + g(m_b^2, \bar{u}m_B^2 + uq^2)(C_3 + C_4 + C_6) \\ & + g(0, \bar{u}m_B^2 + uq^2)(C_3 + 3C_4 + 3C_6) \\ & \left. - \frac{2}{3}(C_3 - C_5 - 15C_6)] + \frac{8C_8^{eff}}{\bar{u} + uq^2/m_B^2} \right\}, \end{aligned} \quad (3.8)$$

where Q_q is the electric charge of spectator quark in the B meson ($q = u, d$). The function $t_{||}(u, m_q)$ convoluted with the B -meson DA ϕ_B^+ arises from the two diagrams in Fig. 3(b) where the virtual photon is emitted from the quark loop. We recalculated and confirmed the resulting expression for $t_{||}(u, m_q)$ presented in Eq. (28) of [8]. In the remaining nonfactorizable diagrams where the virtual photon is emitted from the quarks of the initial or final meson, only the DA ϕ_B^- contributes. Furthermore, we compared the above expression with the dedicated sum rule calculation. To this end, a correlation function with B -meson DA's and kaon interpolating current was introduced where the internal quark loop with the virtual photon emission was inserted. The resulting LCSR reproduces the QCD factorization expression (3.6) if two conditions are satisfied: (1) the asymptotic kaon

DA $\varphi_K(u) = 6u(1-u)$ is substituted in (3.6) and (2) in LCSR the leading-order two-point QCD sum rule for the kaon decay constant is used ².

The factorization formula (3.6) by construction [8] only includes the leading power in the heavy-quark limit. We expect that LCSR can be more advantageous in assessing the power-suppressed corrections to this contribution. Note that in the factorization approach these corrections involve convolutions of the B -meson DA's with higher-twist kaon DAs and generally suffer from end-point divergences. In the LCSR framework, albeit technically more involved, the off-shell correlation function is used where only the B -meson DAs enter.

3.5 Weak annihilation

For this contribution shown in Fig. 5 we use the same approximation as in [8], employing the LO factorization formula

$$\mathcal{H}_{nonf,WA}^{(BK)}(q^2) = \frac{1}{8N_c} \frac{f_B f_K m_b}{m_B^2} \sum_{\pm} \int \frac{d\omega}{\omega} \phi_B^{\pm}(\omega) \int_0^1 du \varphi_K(u) T_{\pm}^{(0)}(u, \omega). \quad (3.9)$$

The hard-scattering kernels $T_{\pm}^{(0)}(u, \omega)$ are given by

$$\begin{aligned} T_+^{(0)}(u, \omega) &= 0, \\ T_-^{(0)}(u, \omega) &= e_q \frac{m_B \omega}{m_B \omega - q^2} \frac{4m_B}{m_b} (C_3 + 3C_4). \end{aligned} \quad (3.10)$$

The leading-power contribution – as well known – originates from the virtual photon emitted from the light-spectator quark inside the B -meson. The other three diagrams in Fig. 5(a) are essential to ensure the e.m. current conservation. As noticed in [8], the weak annihilation diagrams develop an end-point singularity when the invariant mass of lepton pair becomes soft, $q^2 \sim \Lambda_{QCD}^2$. Hence working at large spacelike q^2 we avoid this problem. Radiative corrections to the weak annihilation diagrams (one of them shown in Fig. 5(b)) involving hard gluons are neglected since they have an additional $O(\alpha_s)$ suppression. Note that a soft-gluon emission accompanied by weak annihilation apparently cannot be described by the above factorization formula but instead can be studied using LCSR's. Since there is yet additional power suppression involved we will not dwell on this problem here, expecting that altogether the above factorization formula provides a reasonable estimate of this suppressed effect.

3.6 Power counting

Concluding this section, let us discuss the power counting of separate contributions to the nonlocal amplitude $\mathcal{H}^{(BK)}(q^2)$ considered above. As a reference scaling behaviour we take the $m_b \rightarrow \infty$ limit of the dominant factorizable contributions to $B \rightarrow K \ell^+ \ell^-$ amplitude (2.2) which are determined by the $B \rightarrow K$ form factors. Importantly, the large spacelike scale $|q^2| \gg \Lambda_{QCD}^2$ introduced in our calculation does not scale with m_b , hence it does

² Similar correspondence was found [19] between the LCSR for the $B \rightarrow \pi$ form factor in soft-collinear effective theory and the factorization formula for the hard-collinear spectator contribution to the same form factor.

not influence the familiar scaling behavior of the form factors in the large hadronic recoil region: $f_{BK}^+ \sim f_{BK}^T \sim 1/m_b^{3/2}$. This behaviour follows from the power counting in LCSR's with B -meson DA's for these form factors, as well as from the alternative LCSRs with light meson (pion and kaon) DA's (see e.g.,[30] for a detailed discussion). Note that in the numerical calculation here we use the $B \rightarrow K$ form factors [9] from the LCSR's with kaon DA's calculated at finite m_b , hence beyond the heavy-mass limit.

Turning to $\mathcal{H}^{(BK)}(q^2)$, we notice that the factorizable contributions (3.1) and (3.3) reveal the same power counting $\sim 1/m_b^{3/2}$, since the coefficient functions stemming from the loops can only introduce a logarithmic dependence on the heavy mass scale. The scaling of the nonfactorizable soft-gluon contribution (3.5) is less trivial; it can be obtained from the heavy-quark limit of the LCSR for the hadronic matrix element $\tilde{\mathcal{A}}(m_q^2, q^2)$ given in Eq.(4.8) in [9]. The derivation of the heavy-quark limit follows the same procedure as for the form factor LCSR's in [30]. We obtain $\tilde{\mathcal{A}}(m_q^2, q^2) \sim \Lambda_{QCD}^2/(4m_q^2 - q^2) \times O(m_b^{-3/2})$. Furthermore, the power-counting of the nonfactorizable spectator and weak annihilation contributions is directly obtained from the factorization formulae (3.6) and (3.9), respectively. Taking into account the scaling behaviour $f_B \sim 1/m_b^{1/2}$ and the fact that the kernels g and $T_{\pm}^{(1,0)}$ in the leading power are independent of m_b (modulo logarithms) we obtain that both these contributions scale as $O(m_b^{-3/2})$. Note however that numerically they are quite different, the weak annihilation contribution (3.9) being suppressed due to the Wilson coefficients. Finally, the power-counting analysis of the soft-gluon nonfactorizable contribution of O_{8g} presented in the next section reveals an additional $1/m_b^2$ suppression with respect to the universal $1/m_b^{3/2}$ scaling behaviour. Summarizing, the nonlocal amplitude $\mathcal{H}^{(BK)}(q^2)$ has the same leading-power behaviour as the dominant contributions of the $O_{7,9,10}$ operators. The presence of the additional spacelike scale q^2 is crucial because the main nonperturbative correction to this amplitude stemming from the soft-gluon emission from the quark loops, is "protected" by $\sim 1/|q^2|$. The same q^2 -scale plays a role of a regulator in the nonfactorizable spectator and weak annihilation contributions. This important circumstance justifies our approach of calculating the nonlocal amplitude at large spacelike q^2 . Future efforts to improve the adopted approximation, e.g., in the framework of LCSR's, should be invested in calculating the next-to-leading power corrections in $1/q^2$, such as the two soft-gluon emission diagrams.

4. Soft-gluon contribution of the O_{8g} operator

Here we present a calculation of the nonfactorizable effect in $B \rightarrow K\ell^+\ell^-$ due to the soft-gluon emission generated by the gluon-penguin operator O_8 . The diagram in Fig.4(b) schematically represents this effect; important is that the gluon emission is a long-distance effect as opposed to diagrams Fig.4(a,c) where the gluon is absorbed at short distances and can be described by a perturbative propagator. The nonlocal hadronic matrix element

$$i \int d^4x e^{q \cdot x} \langle K(p) | T \{ j_{em}^\mu(x), C_8^{eff} O_{8g}(0) \} | B(p+q) \rangle = [(p \cdot q)q^\mu - q^2 p^\mu] \mathcal{H}_{O_{8g}}^{(BK)}(q^2) \quad (4.1)$$

includes all effects depicted in Fig. 4. As explained in the previous section, the soft-gluon part of this amplitude corresponds to the term in LCSR with the quark-antiquark-gluon

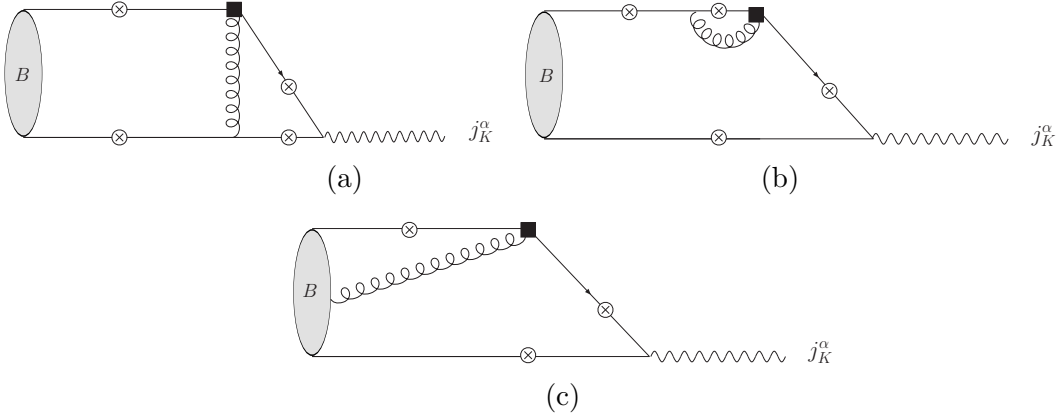


Figure 7: Correlation function used to derive LCSR for the gluon-penguin operator contribution. The diagrams (a),(b) and (c) correspond to the hard-gluon and soft-gluon contributions, respectively.

components of the B meson DA's. The derivation of the sum rule follows the procedure used in [9], and the operator O_{8g} is simpler than the effective nonlocal operator of the soft-gluon emission from the quark loop.

We start from the following correlation function

$$\begin{aligned} \Pi^{\alpha\mu}(p, q) &= i \int d^4y \int d^4x e^{i(p \cdot y + q \cdot x)} \langle 0 | T \{ j_K^\alpha(y), j_{em}^\mu(x), C_8^{eff} O_{8g}(0) \} | B(p+q) \rangle \\ &= ip^\alpha q^\mu \Pi(p^2, q^2) + \dots, \end{aligned} \quad (4.2)$$

where the gluon-penguin operator enters together with the e.m. current and kaon interpolating current $j_K^\alpha = \bar{d}\gamma^\alpha\gamma_5 s$. It is sufficient to consider the single kinematical structure shown on r.h.s., the rest is denoted by ellipses. At the hadronic level, we can express the above correlation function with the help of dispersion relation in the variable p^2 (the kaon-current momentum squared) at fixed q^2 :

$$\Pi^{\alpha\mu}(p, q) = \frac{if_K p^\alpha}{m_K^2 - p^2} [(p \cdot q)q^\mu - q^2 p^\mu] \mathcal{H}_{O_{8g}}^{(BK)}(q^2) + \dots, \quad (4.3)$$

where the ground-state term of the kaon contains the $B \rightarrow K$ transition amplitude we are interested in, and ellipses denote the contributions from the excited and continuum states with the kaon quantum numbers. To derive the sum rule, we match the coefficient at the kinematical structure $\sim p^\alpha q^\mu$ in the above to the invariant amplitude $\Pi(p^2, q^2)$ in (4.2). At sufficiently large $|p^2|$ this correlation function (4.2) can be computed in terms of OPE in terms of B -meson DA's. The gluon field emitted from the operator O_{8g} is either absorbed by one of the virtual quark lines, or enters the B -meson state forming three-particle DA's (see Fig. 7). Only the latter term in OPE interests us here, hence we only have to calculate the diagrams in Fig. 7(c). The diagrams in Figs. 7(a,b) correspond to the hard-gluon contributions already taken into account in terms of QCD factorization and included in the contributions $\mathcal{H}_{fact, NLO}^{(BK)}$ and $\mathcal{H}_{nonf, spect}^{(BK)}$, as described in the previous section.

We decompose the three-particle Fock state of the B meson in terms of four DA's: $\Psi_A(\omega, \xi)$, $\Psi_V(\omega, \xi)$, $X_A(\omega, \xi)$ and $Y_A(\omega, \xi)$, where ω and ξ are the momenta carried by the

light-quark and gluon inside the B -meson. The relevant definitions and ansatz for DA's (see App. B) are the same as the ones used in [9]. After inserting this decomposition in the correlation function we calculate the sum of two diagrams in Fig. 7(c) with the virtual photon emission from b and s quarks; note that the photon emission from the spectator light quark does not contribute to LCSR.

The invariant amplitude $\Pi(p^2, q^2)$ is obtained in the following form:

$$\begin{aligned} \Pi(p^2, q^2) &= \frac{m_b}{8\pi^2} f_B \sum_{n=1,2} \int_0^\infty d\omega \int_0^\infty d\xi \frac{1}{[(p - \omega v)^2 - m_s^2]^n} \\ &\times \left[F_n^{(\Psi A)}(q^2, \omega) \Psi_A(\omega, \xi) + F_n^{(\Psi V)}(q^2, \omega) \Psi_V(\omega, \xi) \right. \\ &\left. + F_n^{(XA)}(q^2, \omega) \bar{X}_A(\omega, \xi) + F_n^{(YA)}(q^2, \omega) \bar{Y}_A(\omega, \xi) \right], \end{aligned} \quad (4.4)$$

where $\bar{X}_A(\omega, \xi) = \int_0^\omega d\eta X_A(\eta, \xi)$, $\bar{Y}_A(\omega, \xi) = \int_0^\omega d\eta Y_A(\eta, \xi)$. The explicit expressions of the coefficient functions $F_n^{(DA)}(q^2, \omega)$ ($n = 1, 2$) multiplying the three-particle B -meson DA's are collected in App. C. To simplify the calculation, we neglect the numerically very small $\sim \xi/m_B$ terms in these functions, hence in the leading power they are independent of the gluon-momentum variable ξ .

Equating two different representations of the correlation function, we obtain

$$\frac{f_K(m_B^2 - m_K^2 - q^2)}{2(m_K^2 - p^2)} \mathcal{H}_{soft, O_8}^{(BK)} + \int_{s_0^h}^\infty ds \frac{\rho^h(s, q^2)}{s - p^2} = \Pi(p^2, q^2). \quad (4.5)$$

In the above, the index ‘‘soft’’ at the amplitude $\mathcal{H}^{(BK)}$ indicates that we only take into account the soft-gluon contribution in the OPE result for the correlation function.

The next important step is to use the quark-hadron duality approximation for the integral over the excited and continuum hadronic states with the kaon quantum numbers:

$$\int_{s_0^h}^\infty ds \frac{\rho^h(s, q^2)}{s - p^2} = \frac{1}{\pi} \int_{s_0^K}^\infty ds \frac{\text{Im}\Pi(s, q^2)}{s - p^2}, \quad (4.6)$$

where the effective threshold s_0^K is introduced. Finally, the Borel transformation is performed to improve the duality approximation and the final sum rule reads:

$$\mathcal{H}_{soft, O_8}^{(BK)}(q^2) = \frac{2e^{m_K^2/M^2}}{f_K(m_B^2 - m_K^2 - q^2)} \frac{1}{\pi} \int_0^{s_0^K} ds e^{-s/M^2} \text{Im}\Pi(s, q^2). \quad (4.7)$$

To obtain the explicit form of the integral on the r.h.s. it is convenient to start from the initial expression (4.4) and use the substitution rules presented in App. C for separate integrals in this expression. These substitutions simultaneously perform the transition to the dispersion form, subtraction of the higher states and Borel transformation.

The soft-gluon contribution of O_{8g} is suppressed by an extra power of $O(\Lambda^2/m_b^2)$ with respect to the factorizable contributions, such as the LO loop contribution. Here Λ is a typical low-mass scale entering B -meson DA's in HQET. The relevant power counting

can be carried out by expanding the sum rule (4.7) at $m_b \rightarrow \infty$. Focussing, e.g., on the contribution of the DA $\Psi_A(\omega, \xi)$ in this sum rule, we obtain after using the substitution rules in App. C:

$$\begin{aligned} \mathcal{H}_{soft, O_8}^{(BK), (\Psi_A)}(q^2) &\sim \frac{m_b f_B}{(m_B^2 - m_K^2 - q^2)} \int_0^{\omega_0} \frac{d\omega}{1 - \omega/m_B} e^{-s/M^2} \\ &\times \int_0^\infty d\xi F_1^{(\Psi_A)}(q^2, \omega) \Psi_A(\omega, \xi) \sim 1/m_b^{7/2}, \end{aligned} \quad (4.8)$$

taking into account that both the threshold parameter $\omega_0 \sim s_0^K/m_B$ and the coefficient function $F_1^{(\Psi_A)}(q^2, \omega)$ scale as $1/m_b$.

5. Nonlocal hadronic effects in timelike region

Collecting the results for separate contributions presented in the previous sections we calculate the nonlocal hadronic amplitude defined in (2.3) at $q^2 < 0$:

$$\begin{aligned} \mathcal{H}^{(BK)}(q^2) &= \mathcal{H}_{fact, LO}^{(BK)}(q^2) + \mathcal{H}_{fact, NLO}^{(BK)}(q^2) + \mathcal{H}_{nonf, spect}^{(BK)}(q^2) \\ &+ \mathcal{H}_{soft, 4q}^{(BK)}(q^2) + \mathcal{H}_{soft, O_8}^{(BK)}(q^2) + \mathcal{H}_{nonf, WA}^{(BK)}(q^2). \end{aligned} \quad (5.1)$$

To access the physical region $4m_\ell^2 < q^2 < (m_B - m_K)^2$ of the $B \rightarrow K\ell^+\ell^-$ decay, following [9], we use hadronic dispersion relation in the channel of virtual photon. Here the following observation is important. The amplitude $\mathcal{H}^{(BK)}(q^2)$ in (5.1) can be decomposed in separate contributions distinguished by the flavour of the quark interacting with the virtual photon via e.m. current. One simply collects all terms in $\mathcal{H}^{(BK)}(q^2)$ that are proportional to the electric charge Q_q of the quark q . This flavour splitting allows one to establish a correspondence between the part of (5.1) with a given Q_q and the hadronic states with the quark content $\bar{q}q$ in the dispersion relation. For example, the part of the amplitude $\mathcal{H}^{(BK)}(q^2)$ proportional to $Q_{u,d}$ (Q_s) is dual to the part of the hadronic dispersion relation containing the vector mesons ρ and ω (ϕ) and excited and continuum states with the same quantum numbers. Here we neglect small mixing effects. Accordingly, the part of the amplitude $\mathcal{H}^{(BK)}(q^2)$ proportional to Q_c generates the vector charmonium states and open charm states in the timelike region. Since $q^2 < m_\Upsilon^2$ in $B \rightarrow K\ell^+\ell^-$, the part of the amplitude proportional to Q_b , only contributes to the nonresonance background in the dispersion relation.

We separate the contributions from different flavors of quarks in (5.1) in the following way:

$$\mathcal{H}^{(BK)}(q^2) = \mathcal{H}_{scb}^{(BK)}(q^2) + \mathcal{H}_{ud}^{(BK)}(q^2), \quad (5.2)$$

so that the first (second) term in the above contains all contributions from the different terms in (5.1) proportional to $Q_{s,c,b}$ ($Q_{u,d}$). The reason why the s, c, b -quark contributions are not separated from each other is that in certain terms included in (5.1) e.g., in $\mathcal{H}_{fact, NLO}^{(BK)}(q^2)$, the virtual photon emissions from b and s quarks are interconnected by gauge invariance. Also the results of [17] used to calculate these contributions do not allow one the separation of the c -quark component. In future, a more detailed flavour separation

can be achieved, performing a dedicated analysis of the NLO two-loop diagrams. Another important point is that the photon emission from the spectator light quarks also contributes to $\mathcal{H}^{(BK)}(q^2)$. Hence, one has to specify the light flavour of the decaying B meson. Our default choice is $\bar{B}^0 \rightarrow \bar{K}^0 \ell^+ \ell^-$. To calculate the isospin asymmetry we will also consider $B^- \rightarrow K^- \ell^+ \ell^-$. In the approximation adopted in this paper, the small CP violation effects are neglected, hence the same results are valid for B^0 and B^+ decays, respectively.

The separate hadronic dispersion relations for the two parts of the decomposition (5.2) are:

$$\mathcal{H}_{scb}^{(BK)}(q^2) = \mathcal{H}_{scb}^{(BK)}(q_0^2) + (q^2 - q_0^2) \left[\sum_{V=\phi, J/\psi, \psi(2S)} \frac{\kappa_V f_V |A_{BVK}| e^{i\varphi_V}}{(m_V^2 - q_0^2)(m_V^2 - q^2 - im_V \Gamma_V^{tot})} + \int_{s_0^h}^{\infty} ds \frac{\rho_{scb}(s)}{(s - q_0^2)(s - q^2 - i\epsilon)} \right]. \quad (5.3)$$

and

$$\mathcal{H}_{ud}^{(BK)}(q^2) = \mathcal{H}_{ud}^{(BK)}(q_0^2) + (q^2 - q_0^2) \left[\sum_{V=\rho, \omega} \frac{\kappa_V f_V |A_{BVK}| e^{i\varphi_V}}{(m_V^2 - q_0^2)(m_V^2 - q^2 - im_V \Gamma_V^{tot})} + \int_{s_0^h}^{\infty} ds \frac{\rho_{ud}(s)}{(s - q_0^2)(s - q^2 - i\epsilon)} \right], \quad (5.4)$$

In the above, the decay constant of a vector meson V with the polarization vector ϵ_V is defined as: $\langle 0 | j_{em}^\mu | V \rangle = \kappa_V m_V f_V \epsilon_V^\mu$; the coefficients $\kappa_\rho = 1/\sqrt{2}$, $\kappa_\omega = 1/(3\sqrt{2})$, $\kappa_\phi = -1/3$, $\kappa_{J/\psi} = \kappa_{\psi(2S)} = 2/3$ follow from the valence quark content of V . As discussed in [9] one subtraction at q_0^2 guarantees the convergence of the dispersion integrals. We choose $q_0^2 = -1.0 \text{ GeV}^2$ and use the calculated result to fix the subtraction terms $\mathcal{H}_{scb,ud}^{(BK)}(q_0^2)$. The advantage of the flavour separation done above is that the suppressed part of the nonlocal amplitude, $\mathcal{H}_{ud}^{(BK)}(q^2 < 0)$, has its own dispersion relation, allowing one a more accurate estimate of contributions with ρ, ω quantum numbers in the timelike region, which otherwise would have been hidden under the dominant contributions of charmonium states.

The residues of vector meson poles in both dispersion relations (5.3) and (5.4) contain amplitudes A_{BVK} of the nonleptonic decays $B \rightarrow VK$. Final-state strong rescattering is taken into account by the phases attributed to each amplitude³. The $B \rightarrow VK$ decays are well measured, allowing one to extract the absolute values of their amplitudes. The relative phases of these amplitudes are unknown and they may considerably influence the pattern of vector meson contributions in the dispersion relations. Note that the absolute values $|A_{BVK}|$ extracted from the experiment deviate from their naive factorization estimates obtained multiplying f_V with the combination of Wilson coefficients and the $B \rightarrow K$ form factor. These deviations are considerable for $V = J/\psi, \psi(2S)$, revealing large non-factorizable effects in $B \rightarrow J/\psi K, \psi(2S)K$, they are somewhat smaller for the decays into

³As discussed above, these phases are related to the discontinuities in the second variable $(p + q)^2$. In this sense the dispersion relations we are considering here can be interpreted as a double-dispersion representations for the amplitude $\mathcal{H}^{(BK)}((p + q)^2, q^2)$, where each amplitude A_{BVK} is itself expressable in a form of single dispersion relation over $(p + q)^2$.

light vector mesons. Altogether, the dispersion relations (5.3) and (5.4) contain too many hadronic degrees of freedom to be fixed and/or constrained solely from the matching of the r.h.s. with the result of the calculation at negative q^2 . Therefore, following the approach advocated in [9] we fix the absolute values of residues in both dispersion relations, employing experimental data on the decay constants and nonleptonic decay amplitudes. The main difference between the relations considered in [9] and here is that, in addition to the contributions of charmonium states, we also include the contributions of light vector mesons employing the data on $B \rightarrow \phi K$ and $B \rightarrow \rho(\omega)K$ partial widths. Importantly, the data currently accumulated in [20, 21] allow one to fix the decay amplitudes for both \bar{B}^0 and B^- mesons separately, which is particularly important for the evaluation of the isospin asymmetry.

After fixing the residues of the lowest resonance poles in both dispersion relations (5.3) and (5.4), they still contain a significant amount of unknown hadronic degrees of freedom from higher states, accumulated in the integrals over spectral densities. Note that the integral in (5.3) contains the contributions of excited ϕ -resonances and continuum states with the same quantum numbers, as well as the contributions of all vector charmonium states and open charm-anticharm states above the threshold $s = 4m_D^2$. The integral in (5.4) in its turn, accumulates excited and continuum states with the ρ, ω quantum numbers. At very large s , approaching the B_s^* meson mass squared the $\bar{b}s$ states contribute in both integrals. At low and intermediate q^2 the presence of these states is signaled (at least in the factorizable part of $\mathcal{H}^{(BK)}(q^2)$) by the growth of the $B \rightarrow K$ form factor. The fit of the dispersion relation to the calculation result at negative q^2 will introduce important constraints on the hadronic integrals entering dispersion relations. However, in order to perform a continuation to positive q^2 one needs to parametrize these integrals in terms of a certain ansatz.

Let us first concentrate on the dominant part of the amplitude parametrized by the hadronic dispersion relation (5.3). Note that the region of q^2 we are interested in, is located below the open charm threshold $4m_D^2$. The only (subdominant) contribution in this region to the spectral density $\rho_{scb}(s)$ originates from the superposition of $\bar{s}s$ states starting from ϕ meson and including its excitations and multiparticle states, such as $\bar{K}K$ with $J^P = 1^-$. The ansatz used in QCD sum rules [22] to describe the $\bar{s}s$ -channel with vector quantum numbers is the ϕ -meson pole combined with the continuum, the latter approximated by the quark-parton duality with an effective threshold. This motivates us to replace the spectral density by the following ansatz:

$$\rho_{scb}(s)\theta(s - s_0^h) = \frac{1}{\pi}\text{Im}\mathcal{H}_{scb}^{BK}(s)\theta(s - s_0^\phi), \quad (5.5)$$

where the effective threshold s_0^ϕ is determined from the QCD sum rule in the ϕ channel. The simplest choice for the r.h.s. is to approximate it with the LO factorizable part $\mathcal{H}_{fact,LO,s}^{BK}$ where the index s indicates that only the part proportional to Q_s is taken in (3.1). The spectral density is then reduced to the imaginary part of the s -quark loop function (3.2) multiplied by the $B \rightarrow K$ form factor. Note that in this case we adopt a stronger assumption of local duality, rather than the semi-local duality used in QCD sum

rules. Also at $s < 4m_D^2$, that is within the validity region for LCSR, the calculated form factor can still be used. We therefore subdivide the integral in the dispersion relation (5.3) in two parts and adopt the approximation (5.5) for the interval $s_0^\phi < s < 4m_D^2$. In addition, the imaginary part of the integral at $q^2 > s_0^\phi$ is modified by introducing an effective width factor in the denominator, replacing $s - q^2 - i\epsilon \rightarrow s - q^2 - i\sqrt{s} \Gamma_{eff}(s)$. The dependence of this width factor on s is taken as $\Gamma_{eff}(s) = \gamma\sqrt{s}\Theta(s - 4m_K^2)$, following the resonance model adopted for the timelike form factors in [23] where the universal value $\gamma = 0.2$ was derived from the spectrum of light vector mesons. The step-function accounts for the kinematical limit where the width vanishes.

In the remaining integral from $4m_D^2$ to infinity, the spectral density $\rho_{scb}(s)$ cannot be simply parametrized because it contains a complicated superposition of four hadronic components: 1) broad charmonium resonances and open-charm continuum states (the dominant contribution), 2) the ‘‘tail’’ of $\bar{s}s$ states, 3) the states with B_s^* quantum numbers and 4) the $\bar{b}b$ states corresponding to the photon emission from b quark. Note however, that in the region of our interest $q^2 < 4m_D^2$ (practically, below the J/ψ mass), this integral has no singularities and can be represented as a generic series expansion in powers of $q^2/4m_D^2$. An alternative is to perform a usual $q^2 \rightarrow z$ transformation and to use the z -expansion. As a default model we use a rather simple approximation

$$\int_{4m_D^2}^{\infty} ds \frac{\rho_{scb}(s)}{(s - q_0^2)(s - q^2 - i\epsilon)} = a_{scb} + b_{scb} \frac{q^2}{4m_D^2}, \quad (5.6)$$

where a_{scb} and b_{scb} are unknown complex constants.

Turning to the second dispersion relation (5.4), we use a similar approximation for the spectral density:

$$\rho_{ud}(s)\theta(s - \tilde{s}_0^h) = \frac{1}{\pi} \text{Im} \mathcal{H}_{ud}^{BK}(s)\theta(s - s_0^\rho), \quad (5.7)$$

where s_0^ρ is the effective threshold, typical for the QCD sum rules in the ρ channel. Accordingly, the integral over large s is represented similar to (5.6) with the two additional complex parameters a_{ud} and b_{ud} . For the sake of uniformity we put the lower limit of this integral to the same value $4m_D^2$.

After parametrizing the integrals over the spectral densities, the dispersion relations (5.3) and (5.4) are fitted to the results for $\mathcal{H}_{scb}^{BK}(q^2)$ and $\mathcal{H}_{ud}^{BK}(q^2)$ respectively, at negative q^2 . The fitted parameters are the coefficients a_{scb}, b_{scb} in the expansion of the integral (5.6) and a_{ud}, b_{ud} for the corresponding integral for u, d quark states. After that, the two dispersion relations are added together and continued to timelike q^2 resulting in the desired nonlocal amplitude $\mathcal{H}^{BK}(q^2)$ for $B \rightarrow K\ell^+\ell^-$ decay. To assess the dependence on the parametrization of the dispersion relations, apart from the default parametrization of the dispersion integrals described above, we also considered three alternative versions: (I) the integral (5.6) is replaced with an effective pole as it was done in [9]; (II) a generic z -series parametrization for the integral over higher states (5.6) is used, and (III) as an extreme choice only the dominant J/ψ and $\psi(2S)$ states are left in the dispersion relation with no flavour-splitting applied.

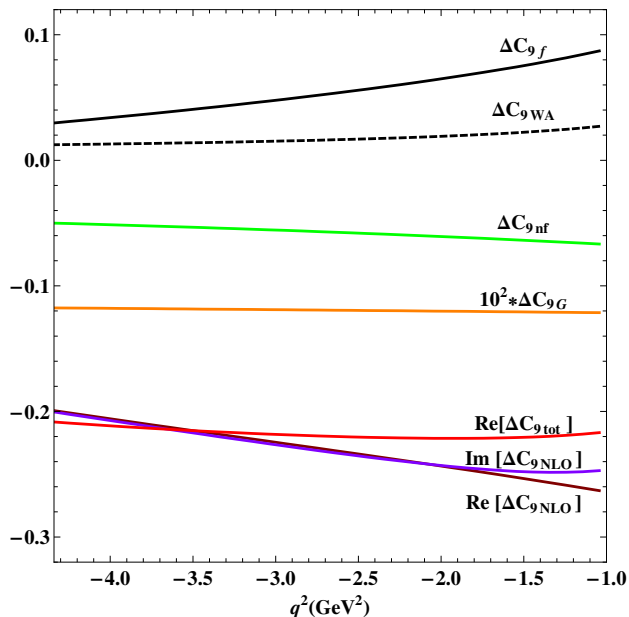


Figure 8: Nonlocal hadronic amplitude in $B \rightarrow K\ell^+\ell^-$, expressed in terms of the correction to C_9 , calculated at $q^2 < 0$ for the central values of the input. The separate contributions are from the factorizable quark loops (ΔC_{9f} , black), weak annihilation (ΔC_{9WA} , dashed black), soft-gluon nonfactorizable emission (ΔC_{9nf} , green), soft-gluon emission from O_{8g} operator (ΔC_{9G} , multiplied by 10^2 , orange), real part of NLO hard-gluon effects ($\text{Re}[\Delta C_{9NLO}]$, brown), total real part ($\text{Re}[\Delta C_{9tot}]$, red), imaginary part of NLO hard-gluon effects ($\text{Im}[\Delta C_{9NLO}]$, violet).

6. Numerical results

We start with the numerical evaluation of the amplitude (5.1) in the region $q^2 < 0$. The same input as in [9] is adopted, where one can find more details. In particular, since the calculation is done at spacelike momentum transfer, it is more appropriate to use the $\overline{\text{MS}}$ quark masses, for which we adopt the following intervals: $m_s(2 \text{ GeV}) = (98 \pm 16) \text{ MeV}$, $m_c(m_c) = (1.29 \pm 0.03) \text{ GeV}$ and $m_b(m_b) = (4.164 \pm 0.025) \text{ GeV}$. The functional form of B -meson DA's entering the factorization formulae and LCSR's is specified in App. B. We use the interval $f_B = 180 \pm 30 \text{ MeV}$ for the decay constant, $\lambda_B(1 \text{ GeV}) = 460 \pm 110 \text{ MeV}$ for the inverse moment and $\lambda_E(1 \text{ GeV}) = \sqrt{3/2} \lambda_B(1 \text{ GeV})$ for the parameter entering the 3-particle DA's. For the kaon decay constant we use [20] $f_K = 159.8 \pm 1.4 \pm 0.44 \text{ MeV}$ and for the Gegenbauer moments of the kaon DA: $a_1^K(1 \text{ GeV}) = 0.10 \pm 0.04$, $a_2^K(1 \text{ GeV}) = 0.25 \pm 0.15$. Finally, in LCSR with the kaon interpolating current the Borel parameter and effective duality threshold are taken as $M^2 = 1.0 \pm 0.25 \text{ GeV}^2$ and $s_0^K = 1.05 \text{ GeV}^2$, respectively. The default value of the renormalization scale is $\mu = 3.0 \text{ GeV}$, so that $\alpha_s(3 \text{ GeV}) = 0.252$, and the scale is then varied within $2.5 \text{ GeV} < \mu < 4.5 \text{ GeV}$.

For the $B \rightarrow K$ form factors the predictions from LCSR with kaon DA's are used. They are presented in the App. B of [9], in particular, the normalization of the vector and tensor form factors are given by $f_{BK}^+(0) = 0.34_{-0.02}^{+0.05}$, and $f_{BK}^T(0) = 0.39_{-0.03}^{+0.05}$, respectively.

In the contributions calculated using QCD factorization approach we adopt a universal $B \rightarrow K$ form factor $\xi_{BK}(q^2)$ which is set equal to $f_{BK}^+(q^2)$, neglecting the small difference between tensor and vector form factors.

According to (2.4), the result for $\mathcal{H}^{(BK)}(q^2 < 0)$ is normalized to the form factor, yielding a correction to the Wilson coefficient C_9 . Separate contributions to this correction are plotted in Fig. 8 for the central values of the input. Numerically, in the real part of $\Delta C_9^{(BK)}(q^2)$ there are substantial cancellations between separate contributions, and the soft-gluon nonfactorizable part plays an important role as already observed in [9]. Altogether, the real and imaginary parts of $\Delta C_9^{(BK)}(q^2 < 0)$ – the latter generated by the NLO hard-gluon effects – reach the level of a few percent of the short-distance coefficient C_9 .

To assess the impact of nonlocal hadronic effects on the observables in $B \rightarrow K\ell^+\ell^-$, we turn now to the numerical analysis of the dispersion relations, allowing us to smoothly continue these effects into the physical region $q^2 > 0$. To this end, we follow the procedure described in the previous section, splitting $\mathcal{H}^{(BK)}(q^2)$ according to (5.2), and fitting the functions $\mathcal{H}_{scb}^{(BK)}(q^2)$ and $\mathcal{H}_{ud}^{(BK)}(q^2)$ in the region $-4m_c^2 < q^2 < -1.0 \text{ GeV}^2$ to the two dispersion relations (5.3) and (5.4), respectively. In these relations, the absolute values of the nonleptonic $B \rightarrow VK$ amplitudes, together with the decay constants of vector mesons entering the residues of the resonance poles, are extracted from the experimental data [20] on the $B \rightarrow VK$ and $V \rightarrow \ell^+\ell^-$ widths. These parameters are collected in Table 1.

Vector meson	ρ	ω	ϕ	J/ψ	$\psi(2S)$
f_V	221_{-1}^{+1}	195_{-4}^{+3}	228_{-2}^{+2}	416_{-6}^{+5}	297_{-2}^{+3}
$ A_{\bar{B}^0 V \bar{K}^0} $	$1.3_{-0.1}^{+0.1}$	$1.4_{-0.1}^{+0.1}$	$1.8_{-0.1}^{+0.1}$	$33.9_{-0.7}^{+0.7}$	$44.4_{-2.2}^{+2.2}$
$ A_{B^- V K^-} $	$1.2_{-0.1}^{+0.1}$	$1.5_{-0.1}^{+0.1}$	$1.8_{-0.1}^{+0.1}$	$35.6_{-0.6}^{+0.6}$	$42.0_{-1.2}^{+1.2}$

Table 1: Decay constants of vector mesons and amplitudes of $B \rightarrow VK$ decays (all in MeV) calculated from the experimental data [20].

Furthermore, the integrals over the spectral functions of higher states in (5.3) and (5.4) are subdivided in two parts. The integral below $4m_D^2$ is parametrized employing the local duality approximation with the effective thresholds $s_0^\phi = 1.95 \text{ GeV}^2$ in (5.5) and $s_0^\rho = 1.5 \text{ GeV}^2$ in (5.7), whereas for the remaining integrals above $4m_D^2$ the polynomial approximations in the form (5.6) are used. In (5.3) the phases of J/ψ and $\psi(2S)$ contributions are varied independently at $-\pi < \varphi_{J/\psi}, \varphi_{\psi(2S)} \leq \pi$ and the ϕ contribution is taken real. For each combination of the phases $\varphi_{J/\psi}$ and $\varphi_{\psi(2S)}$ the fit of the complex parameters a_{scb} and b_{scb} is repeated. The best fit is obtained when a destructive interference between the J/ψ and $\psi(2S)$ terms in (5.3) takes place, as observed before in [9]. The second dispersion relation (5.4) is treated in a similar way. The phases and fitted parameters are collected in Table 2. Substituting them in the dispersion relations, and continuing the latter to $q^2 > 0$

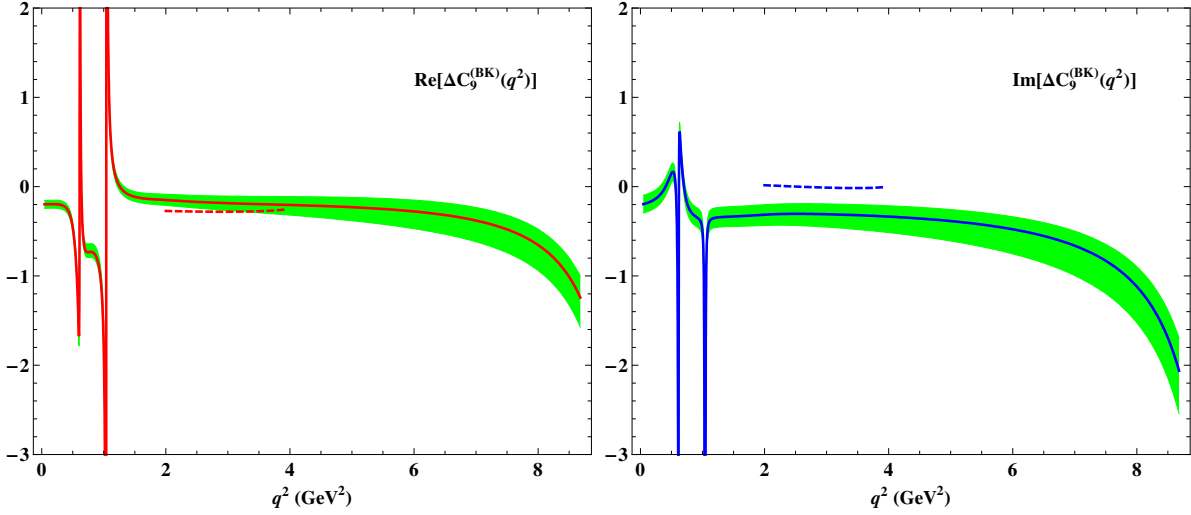


Figure 9: The effective correction $\Delta C_9^{BK}(q^2)$ in the physical region of $B \rightarrow K\ell^+\ell^-$: the red (blue) solid curve corresponds to the real (imaginary) part obtained from the hadronic dispersion relation, fitted to the QCD calculation at $q^2 < 0$ (central input, default parametrization). The shaded areas indicate the uncertainties. The dashed curves correspond to the prediction of QCD factorization obtained with same input.

we finally obtain a numerical result for the nonlocal hadronic amplitude $\mathcal{H}^{BK}(q^2)$ in the physical region.

The resulting effective correction $\Delta C_9^{BK}(q^2 > 0)$ is plotted in Fig. 9 in the region of large hadronic recoil, up to $q^2 \sim m_{J/\psi}^2$. At $q^2 \leq m_\phi^2$ the behavior of $\Delta C_9^{BK}(q^2)$ reflects the presence of light vector resonances. In the same figure we compare our result with the result for ΔC_9^{BK} directly calculated at $q^2 > 0$, using the same approach and approximation as in [8]. This comparison is possible in a restricted region, $2.0 \text{ GeV}^2 \leq q^2 \leq 4.0 \text{ GeV}^2$, above the light resonances and sufficiently below the $\bar{c}c$ -quark threshold. In this region, the real parts $\Delta C_9^{BK}(q^2)$ obtained from our dispersion approach and from the direct calculation are in agreement within uncertainties, whereas the imaginary parts deviate from each other.

The uncertainties shown in Fig. 9 are estimated by varying each input parameter involved in the calculation of $\Delta C_9^{BK}(q^2 < 0)$ and then recalculating $\Delta C_9^{BK}(q^2 > 0)$ from the dispersion relation with the modified input. The resulting individual deviations of $\Delta C_9^{BK}(q^2 > 0)$ are then added in quadrature. Furthermore, we repeat the fit of the dispersion relations for the three alternative parametrizations of the dispersion integrals

$\varphi_{J/\psi}$	$\varphi_{\psi(2S)}$	$ a_{scb} [\text{GeV}^{-2}]$	$\text{Arg}[a_{scb}]$	$ b_{scb} [\text{GeV}^{-2}]$	$\text{Arg}[b_{scb}]$
-2.14	0.77	1.40×10^{-5}	0.69	1.37×10^{-4}	0.86
φ_ρ	φ_ω	$ a_{ud} [\text{GeV}^{-2}]$	$\text{Arg}[a_{ud}]$	$ b_{ud} [\text{GeV}^{-2}]$	$\text{Arg}[b_{ud}]$
0.64	-2.50	2.74×10^{-5}	-2.13	5.75×10^{-5}	-2.07

Table 2: Parameters of the dispersion relations (5.3) and (5.4) obtained from the fit to the amplitudes $\mathcal{H}_{scb}^{(BK)}$ and $\mathcal{H}_{ud}^{(BK)}$ at $q^2 < 0$ for the central values of the input.

Table 3: The effective correction to the coefficient C_9 at different q^2 .

q^2 (GeV ²)	Re[$\Delta C_9^{BK}(q^2)$]	Im[$\Delta C_9^{BK}(q^2)$]
1.5	$-0.11^{+0.06}_{-0.05}$	$-0.33^{+0.11}_{-0.11}$
2.0	$-0.15^{+0.07}_{-0.06}$	$-0.31^{+0.11}_{-0.12}$
2.5	$-0.17^{+0.07}_{-0.07}$	$-0.30^{+0.11}_{-0.13}$
3.0	$-0.18^{+0.08}_{-0.08}$	$-0.31^{+0.12}_{-0.14}$
3.5	$-0.20^{+0.09}_{-0.10}$	$-0.32^{+0.12}_{-0.16}$
4.0	$-0.21^{+0.09}_{-0.12}$	$-0.34^{+0.12}_{-0.18}$
4.5	$-0.22^{+0.10}_{-0.13}$	$-0.36^{+0.13}_{-0.20}$
5.0	$-0.23^{+0.11}_{-0.15}$	$-0.39^{+0.13}_{-0.22}$
5.5	$-0.25^{+0.12}_{-0.17}$	$-0.42^{+0.13}_{-0.25}$
6.0	$-0.28^{+0.13}_{-0.19}$	$-0.48^{+0.14}_{-0.28}$
6.5	$-0.32^{+0.14}_{-0.22}$	$-0.55^{+0.15}_{-0.30}$
7.0	$-0.38^{+0.15}_{-0.24}$	$-0.66^{+0.16}_{-0.33}$
7.5	$-0.48^{+0.16}_{-0.26}$	$-0.83^{+0.18}_{-0.37}$
8.0	$-0.65^{+0.18}_{-0.29}$	$-1.12^{+0.22}_{-0.40}$
8.5	$-1.01^{+0.21}_{-0.32}$	$-1.69^{+0.31}_{-0.45}$
9.0	$-2.02^{+0.34}_{-0.38}$	$-3.29^{+0.57}_{-0.56}$

(I)-(III) specified at the end of the previous section. We interpret the difference between $\Delta C_9^{BK}(q^2 > 0)$ obtained with the default parametrization and the one in the model III (which only contains J/ψ and $\psi(2S)$ resonances) as the “systematic” uncertainty of our approach and include it in the uncertainty budget. As an example, we present the correction to C_9 calculated at one particular value of dilepton mass:

$$\text{Re}[\Delta C_9^{BK}(q^2 = 4 \text{ GeV}^2)] = -0.21^{+0.03}_{-0.04} \left|_{\lambda_B} \begin{array}{c} +0.00 \\ -0.10 \end{array} \right|_{a_1^K} \begin{array}{c} +0.08 \\ -0.00 \end{array} \left|_{\mu} \begin{array}{c} +0.02 \\ -0.01 \end{array} \right|_{f_{BK}^+(0)} \begin{array}{c} +0.02 \\ -0.06 \end{array} \left|_{\text{sys.}} \right. , \quad (6.1)$$

$$\text{Im}[\Delta C_9^{BK}(q^2 = 4 \text{ GeV}^2)] = -0.34^{+0.05}_{-0.07} \left|_{\lambda_B} \begin{array}{c} +0.01 \\ -0.12 \end{array} \right|_{a_1^K} \begin{array}{c} +0.08 \\ -0.07 \end{array} \left|_{a_2^K} \begin{array}{c} +0.06 \\ -0.03 \end{array} \right|_{\mu} \begin{array}{c} +0.05 \\ -0.02 \end{array} \left|_{f_{BK}^+(0)} \begin{array}{c} +0.02 \\ -0.04 \end{array} \right|_{\text{sys.}} ,$$

where all significant ($> \pm 5\%$) uncertainties are shown separately. As expected, the dependence on the $B \rightarrow K$ form factor is inessential. Here, we assume a fixed uncertainty for $B \rightarrow K$ form factors stemming from LCSR and neglect possible correlations when varying the rest of the input. For convenience, we also present the numerical intervals for $\Delta C_9^{BK}(q^2)$ in the region $1.5 \text{ GeV}^2 < q^2 < 9.0 \text{ GeV}^2$ in Table 3. They have to be compared with $C_9 \simeq 4.0 - 4.5$ (see App. A). The magnitude of $\Delta C_9^{BK}(q^2)$ remains in the ballpark of $\sim 10\%$ of C_9 at small and intermediate q^2 and grows approaching the charmonium region. We refrain from quoting $\Delta C_9^{BK}(q^2)$ in the region between J/ψ and $\psi(2S)$ where the “systematic” uncertainty caused by the parameterization of dispersion relation is rather large.

7. Observables in $B \rightarrow K\ell^+\ell^-$

Substituting the numerical results for $\mathcal{H}^{(BK)}(q^2)$ to the amplitude (2.2), we calculate the differential width of $\bar{B}^0 \rightarrow \bar{K}^0\mu^+\mu^-$ in the region $4m_\mu^2 < q^2 < 4m_D^2$ (see Fig. 10). Integrating over the typical intervals of dilepton-mass squared (bins) selected in the experiments, we present the resulting partial widths in Table 4, in comparison with the available measurements. In order to illustrate the origin of the quoted uncertainties, we present them separately for one of the bins:

$$\begin{aligned}
 & \int_{1.0 \text{ GeV}^2}^{6.0 \text{ GeV}^2} dq^2 \frac{dBR(\bar{B}^0 \rightarrow \bar{K}^0\mu^+\mu^-)}{dq^2} \\
 &= \left(1.76 \begin{array}{c} +0.58 \\ -0.21 \end{array} \Big|_{f_{BK}^+(0)} \begin{array}{c} +0.16 \\ -0.09 \end{array} \Big|_{slope} \begin{array}{c} +0.01 \\ -0.01 \end{array} \Big|_{\mu} \begin{array}{c} +0.01 \\ -0.02 \end{array} \Big|_{syst.} \right) \times 10^{-7}, \quad (7.1)
 \end{aligned}$$

where the remaining individual uncertainties smaller than 1% are not shown. As opposed to $\Delta C_9^{(BK)}$, the theoretical uncertainty of the width mainly originates from the normalization of the form factor f_{BK}^+ . Our predictions for the partial widths of $\bar{B}^0 \rightarrow \bar{K}^0\ell^+\ell^-$ in Table 4 are somewhat larger than the results of the most recent LHCb measurement [4] of $B^- \rightarrow K^-\ell^+\ell^-$.

Table 4: $dBR(B \rightarrow K\mu^+\mu^-)/dq^2$ integrated over $[q_{min}^2, q_{max}^2]$ in units of 10^{-7} .

$[q_{min}^2, q_{max}^2]$ GeV ²	Belle [5]	CDF [7]	LHCb [3]	LHCb [4]	this work
[0.05, 2.0]	$0.81^{+0.18}_{-0.16} \pm 0.05$	$0.33 \pm 0.10 \pm 0.02$	$0.21^{+0.27}_{-0.23}$	$0.56 \pm 0.05 \pm 0.03$	$0.71^{+0.22}_{-0.08}$
[2.0, 4.3]	$0.46^{+0.14}_{-0.12} \pm 0.03$	$0.77 \pm 0.14 \pm 0.05$	$0.07^{+0.25}_{-0.21}$	$0.57 \pm 0.05 \pm 0.02$	$0.80^{+0.27}_{-0.11}$
[4.3, 8.68]	$1.00^{+0.19}_{-0.08} \pm 0.06$	$1.05 \pm 0.17 \pm 0.07$	1.2 ± 0.3	$1.00 \pm 0.07 \pm 0.04$	$1.39^{+0.53}_{-0.22}$
[1.0, 6.0]	$1.36^{+0.23}_{-0.21} \pm 0.08$	$1.29 \pm 0.18 \pm 0.08$	$0.65^{+0.45}_{-0.35}$	$1.21 \pm 0.09 \pm 0.07$	$1.76^{+0.60}_{-0.23}$

In addition, we also calculated the (CP averaged) isospin asymmetry in $B \rightarrow K\ell^+\ell^-$ defined as

$$a_I^{(0-)}(q^2) = \frac{d\Gamma(\bar{B}_0 \rightarrow \bar{K}_0\ell^+\ell^-)/dq^2 - d\Gamma(B^- \rightarrow K^-\ell^+\ell^-)/dq^2}{d\Gamma(\bar{B}_0 \rightarrow \bar{K}_0\ell^+\ell^-)/dq^2 + d\Gamma(B^- \rightarrow K^-\ell^+\ell^-)/dq^2}, \quad (7.2)$$

In our approach this effect originates from the small differences between the amplitudes of photon emission from the d and u spectator quarks, in the nonfactorizable NLO con-

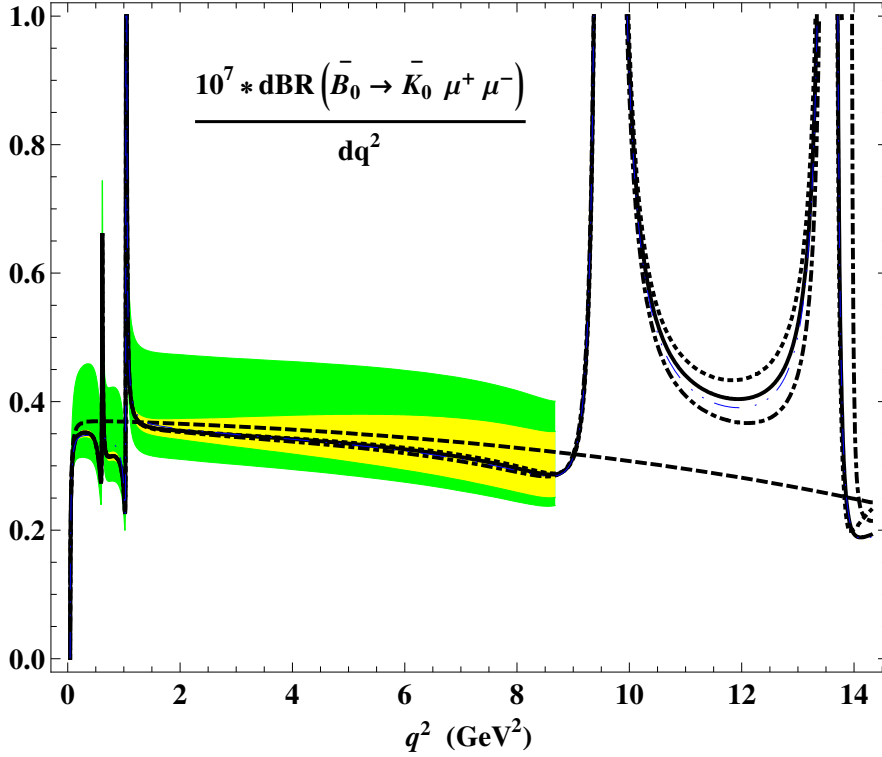


Figure 10: Differential branching fraction of $\bar{B}^0 \rightarrow \bar{K}^0 \mu^+ \mu^-$. The solid line corresponds to the central input and to the default parametrization for the dispersion integrals. The darker (green) and brighter (yellow) shaded area indicates the uncertainties including (excluding) the one from the form factor normalization. The alternative parametrizations I, II and III of the dispersion integrals yield dotted, dash-dotted and thin dash-double-dotted (blue) lines, respectively. The long-dashed line corresponds to the width calculated without nonlocal hadronic effects.

Table 5: Isospin asymmetry calculated from the partial widths of $\bar{B}^0 \rightarrow \bar{K}^0 \ell^+ \ell^-$ and $B^- \rightarrow K^- \ell^+ \ell^-$ integrated over $1.0 < q^2 < 6.0$ GeV².

Belle [5]	BaBar [6]	LHCb [3]	this work
$-0.41^{+0.25}_{-0.20} \pm 0.07$	$-0.41 \pm 0.25 \pm 0.01$	$-0.35^{+0.23}_{-0.27}$	$(-0.4)\% \div (-0.3)\%$

tributions and in the weak annihilation. The result for the differential asymmetry defined above is shown in Fig. 11 and does not exceed a $\pm 4\%$ level within estimated errors. At $q^2 > 2$ GeV² our expectation for the isospin asymmetry in $B \rightarrow K \ell^+ \ell^-$ is in the ballpark of the prediction obtained in [24] for the isospin asymmetry in $B \rightarrow K^* \ell^+ \ell^-$. In Table 5 we present the integrated isospin asymmetry defined similarly to (7.2) but with the partially integrated widths instead of differential widths. This integrated characteristics is expected

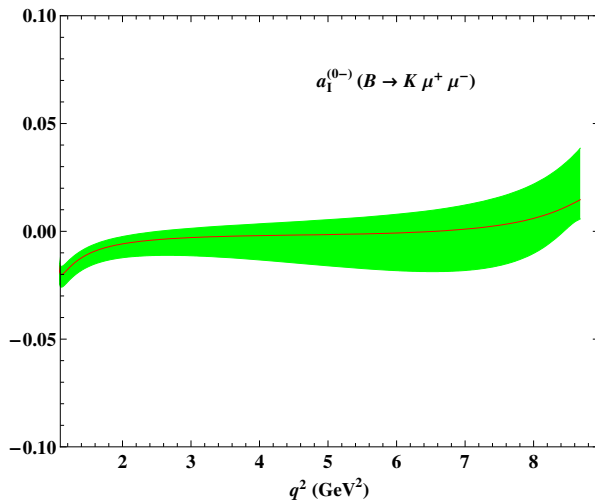


Figure 11: Isospin asymmetry $a_1^{(0-)}(q^2)$ in $B \rightarrow K\ell^+\ell^-$ (the solid curve), the shaded (green) band indicates the uncertainty of our prediction.

to be very small, revealing an intriguing tension with the available experimental measurements presented in the same table. It is important to further improve the accuracy of our prediction. E.g., the calculation presented here assumes isospin symmetry for the $B \rightarrow K$ form factors. This issue deserves a separate study but – having in mind the usual magnitude of isospin violation – it is hard to expect that the deviation of $f_{B^0K^0}^+$ from $f_{B^-K^-}^+$ brings substantial changes in the isospin asymmetry of $B \rightarrow K\ell^+\ell^-$.

Having at hand the SM prediction for the amplitude of $B \rightarrow K\ell^+\ell^-$ it is interesting to investigate the potential influence of new physics in $b \rightarrow s\ell^+\ell^-$ on the observables in this decay. Recent improvement [25] of the upper bound for $BR(B_s \rightarrow \mu^+\mu^-)$ has already put substantial constraints on the new FCNC operators involving pseudoscalar and scalar couplings of the lepton pair. Hence we only consider a generic new physics induced by the two tensor operators:

$$O_T = \frac{\alpha_{em}}{2\pi} (\bar{s}\sigma_{\mu\nu}b) (\bar{l}\sigma^{\mu\nu}l) , \quad O_{T5} = \frac{\alpha_{em}}{2\pi} (\bar{s}\sigma_{\mu\nu}b) (\bar{l}\sigma^{\mu\nu}\gamma_5l) , \quad (7.3)$$

with Wilson coefficients C_T and C_{T5} , respectively.

The $B \rightarrow K\ell^+\ell^-$ width is calculated adding the new operator contributions to the decay amplitude and assuming $C_T = \pm C_{T5}$. As shown in [10], these two parameters are effectively constrained by comparing the measured upper bounds on the inclusive branching fraction $\bar{B} \rightarrow X_s\ell^+\ell^-$ with the SM prediction. Typically one obtains $|C_T| \sim |C_{T5}| < 1.2$. With this constraint, our result for the decay rate of $B \rightarrow K\ell^+\ell^-$, including the new physics contribution and integrated over the interval $1.0 < q^2 < 6.0 \text{ GeV}^2$, reveals a rather small deviation from the SM prediction, at the level of $< 5\%$. The predicted forward-backward asymmetry in $B \rightarrow K\ell^+\ell^-$, emerging due to the new operators (7.3), is plotted in Fig. 12 at $C_T = C_{T5} = 1.2$. This observable can reach at most $-(5 - 10)\%$, being almost independent of q^2 . There are measurements of the forward-backward asymmetry

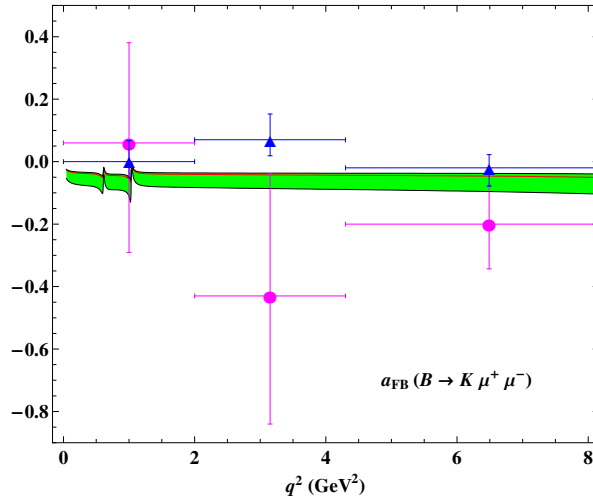


Figure 12: Forward-backward asymmetry in $B \rightarrow K\ell^+\ell^-$ emerging due to new physics contributions of tensor operators with the Wilson coefficients $C_T = C_{T5} = 1.2$. The shaded (green) band indicates the uncertainty of our prediction due to variation of SM parameters. The data points are from the measurement by LHCb [4] (triangles) and Belle [5] (circles).

in $B \rightarrow K\ell^+\ell^-$ by Belle Collaboration [5] and more recently by LHCb Collaboration [4], see Fig. 12. However, these measurements are not yet sensitive to such small effects.

8. Discussion

In this paper, we calculated the nonlocal hadronic contributions to $B \rightarrow K\ell^+\ell^-$ generated by the four-quark and gluon-penguin operators of the effective Hamiltonian, combined with the e.m. emission of the lepton pair. In this calculation the LCSR results for the form factors and for the soft-gluon nonfactorizable effects are used, whereas the hard-gluon effects are approximated employing QCD factorization. We followed the method suggested in [9], combining the QCD results for the nonlocal hadronic matrix elements valid in the region of negative dilepton-mass squared, with the dispersion relations in the physical region. In these relations the residues of the lowest vector mesons are fixed from the data, whereas a nontrivial destructive interference between the dominant J/ψ and $\psi(2S)$ contributions plays an important role. A model ansatz is adopted for the higher state contributions to the dispersion relations, with the parameters fitted to the nonlocal amplitude calculated in QCD.

Our main result is the numerical prediction for the nonlocal hadronic amplitude $\mathcal{H}^{(BK)}(q^2)$ cast in the form of the correction to the Wilson coefficient C_9 . This correction displayed in Table 3 and in Fig. 9 can be used in future phenomenological analysis of the $B \rightarrow K\ell^+\ell^-$ decay. Employing dispersion relation, we avoid unphysical “kinks” in the observables generated by the quark-antiquark production thresholds which appear if one directly uses QCD diagrams in the physical region (see e.g., [26]). Probing alternative parametrizations of the dispersion integrals we argue that the “systematic” uncertainty

introduced by this procedure is inessential in the large hadronic recoil region, practically up to $q^2 = m_{J/\psi}^2$. The approach used here is not applicable at larger values of dilepton mass, especially at $q^2 > 4m_D^2$, where a complicated interference of charmonium resonances and the proximity of the singularities of the $B \rightarrow K$ form factors brings too many hadronic degrees of freedom into play ⁴.

In the large hadronic recoil region, we evaluated the partial width and isospin asymmetry of $B \rightarrow K\ell^+\ell^-$. The impact of nonlocal hadronic contributions on the width is moderate below the charmonium region. The main uncertainty of our prediction in this region stems from the normalization of the $B \rightarrow K$ form factors, leaving a room for improving the accuracy of the SM prediction for $B \rightarrow K\ell^+\ell^-$. In particular, new precise lattice calculations of these form factors combined with updated LCSR results at small q^2 are desirable. In addition, we predict a very small isospin asymmetry in $B \rightarrow K\ell^+\ell^-$, hence, more precise measurements of this observable are needed.

A further improvement of our prediction for the effective correction $\Delta C_9^{(BK)}(q^2)$ is possible along two lines: firstly, achieving more accuracy in QCD calculations at negative q^2 and secondly, with more detailed parametrizations of the dispersion integrals adding the excited vector meson terms. In this respect, dedicated measurements of nonleptonic decays of the type $B \rightarrow V'K$ where V' are radial excitations of ρ, ω, ϕ and the charmonium levels starting from $\psi(3772)$ will be helpful.

The study presented in this paper could be extended to $B \rightarrow K^*\ell^+\ell^-$, for which the charm-loop effect has already been analyzed in [9]. However, calculating the other effects in this process will be more demanding. E.g., the nonlocal hadronic contributions proportional to Q_s such as the ϕ -meson pole will be enhanced at small q^2 , being multiplied by the factor $1/q^2$ from the virtual photon propagator in the amplitude for the transversely polarized K^* meson. To accurately analyze this particular contribution, a separation of $Q_s - Q_b$ component from the Q_c -one is desirable in all three nonlocal hadronic amplitudes $\mathcal{H}_{1,2,3}^{(BK^*)}$ corresponding to the three polarization states of the K^* meson. This demands a dedicated “flavour splitting” of the NLO diagrams calculated in [16, 17] on one hand and a separate dispersion relation with $\bar{s}s$ vector-meson states on the other hand. Also the NLO two-loop diagrams induced by the penguin operators should be included to achieve an adequate accuracy. Altogether, the QCD calculation at negative q^2 and a complete analysis of hadronic dispersion relations for all three invariant amplitudes of $B \rightarrow K^*\ell^+\ell^-$ represents a significantly more challenging task. The nonlocal corrections to C_9 are expected to be numerically larger than for the kaon mode, as already seen from the comparison of charm loop effects for both processes in [9]. Hence, a substantial impact of the nonlocal hadronic effects on $B \rightarrow K^*\ell^+\ell^-$ is anticipated, even in the large hadronic recoil region. Last but not least, as already discussed in the introduction, the fact that K^* has a finite width decaying to $K\pi$, hinders one from the calculation of “pure” $B \rightarrow K^*$ form factors, with

⁴Let us mention that in the low hadronic-recoil region a different method is used [27], based on the local OPE of the nonlocal hadronic amplitudes valid at $q^2 \sim m_b^2 \rightarrow \infty$. Applying this method to $B \rightarrow K^{(*)}\ell^+\ell^-$ decay, one relies on the (quasi)local quark-hadron duality and smallness of power corrections. The connection of the local OPE to the approach used in this paper is an interesting open problem that deserves a dedicated study.

the accuracy achieved for the $B \rightarrow K$ form factors, either on the lattice or with QCD sum rules. New approaches are desirable to calculate the form factors of B -meson transitions to the two-meson system including resonances. Only in this case the theory can meet the challenge of continuously improving experimental measurements of exclusive FCNC B decays.

Acknowledgements

We are thankful to H. Asatrian and C. Greub for useful discussions on their NLO diagram calculation. This work is supported by the German Ministry of Research (BMBF), Contract No. 05H09PSF.

Appendix A: Effective Hamiltonian

Here we list the operators entering the effective Hamiltonian (2.1):

$$\begin{aligned}
O_1 &= (\bar{s}_L \gamma_\rho c_L) (\bar{c}_L \gamma^\rho b_L) , & O_2 &= \left(\bar{s}_L^j \gamma_\rho c_L^i \right) \left(\bar{c}_L^i \gamma^\rho b_L^j \right) , \\
O_3 &= (\bar{s}_L \gamma_\rho b_L) \sum_q (\bar{q}_L \gamma^\rho q_L) , & O_4 &= \left(\bar{s}_L^i \gamma_\rho b_L^j \right) \sum_q \left(\bar{q}_L^j \gamma^\rho q_L^i \right) , \\
O_5 &= (\bar{s}_L \gamma_\rho b_L) \sum_q (\bar{q}_R \gamma^\rho q_R) , & O_6 &= \left(\bar{s}_L^i \gamma_\rho b_L^j \right) \sum_q \left(\bar{q}_R^j \gamma^\rho q_R^i \right) , \\
O_{7\gamma} &= -\frac{e}{16\pi^2} \bar{s} \sigma_{\mu\nu} (m_s L + m_b R) b F^{\mu\nu} , & O_{8g} &= -\frac{g_s}{16\pi^2} \bar{s}_i \sigma_{\mu\nu} (m_s L + m_b R) T_{ij}^a b_j G^{a\mu\nu} , \\
O_9 &= \frac{\alpha_{em}}{4\pi} (\bar{s}_L \gamma_\rho b_L) (\bar{l} \gamma^\rho l) , & O_{10} &= \frac{\alpha_{em}}{4\pi} (\bar{s}_L \gamma_\rho b_L) (\bar{l} \gamma^\rho \gamma_5 l) ,
\end{aligned}$$

where the notations are $q_{L(R)} = \frac{1-(+)\gamma_5}{2} q$ and $L(R) = \frac{1-(+)\gamma_5}{2}$. We use the standard conventions for the operators O_i , except the labeling of O_1 and O_2 is interchanged. The sign convention for $O_{7\gamma}$ and O_{8g} corresponds to the covariant derivative $iD_\mu = i\partial_\mu + eQ_f A_\mu + gT^a A_\mu^a$, where Q_f is the fermion charge. In addition, the convention for the Levi-Civita tensor adopted in this work is $\text{Tr}\{\gamma^\mu \gamma^\nu \gamma^\rho \gamma^\lambda \gamma^5\} = 4i\epsilon^{\mu\nu\rho\lambda}$, $\epsilon^{0123} = -1$. The numerical values of the Wilson coefficients at three different values of the scale μ are listed in the table below [13]:

μ (GeV)	$0.5m_b$	m_b	$1.5m_b$
C_1	1.193	1.117	1.090
C_2	-0.401	-0.267	-0.214
$C_3(\times 10^{-2})$	1.919	1.206	0.931
$C_4(\times 10^{-2})$	-3.964	-2.750	-2.225
$C_5(\times 10^{-2})$	1.041	0.770	0.639
$C_6(\times 10^{-2})$	-5.479	-3.411	-2.637
C_7	-0.370	-0.320	-0.297
C_{8g}	-0.184	-0.166	-0.157
C_9	4.450	4.232	4.029
C_{10}	-4.410	-4.410	-4.410

We also use $|V_{ts}| = 0.0405_{-0.0010}^{+0.0006}$, $|V_{tb}| = 0.999_{-0.00025}^{+0.00043}$ [28] and $\alpha_{em} = 1/129$.

Appendix B: B -Meson Light-cone DA's

In $x^2 = 0$ limit we adopt the following decomposition of the B -to-vacuum matrix element into four independent three-particle DA's (see e.g., [29]):

$$\begin{aligned} \langle 0 | \bar{q}_\alpha(x) G_{\lambda\rho}(ux) h_{v\beta}(0) | \bar{B}^0(v) \rangle &= \frac{f_B m_B}{4} \int_0^\infty d\omega \int_0^\infty d\xi e^{-i(\omega+u\xi)v \cdot x} \\ &\times \left[(1 + \not{v}) \left\{ (v_\lambda \gamma_\rho - v_\rho \gamma_\lambda) \left(\Psi_A(\omega, \xi) - \Psi_V(\omega, \xi) \right) - i\sigma_{\lambda\rho} \Psi_V(\omega, \xi) \right. \right. \\ &\left. \left. - \left(\frac{x_\lambda v_\rho - x_\rho v_\lambda}{v \cdot x} \right) X_A(\omega, \xi) + \left(\frac{x_\lambda \gamma_\rho - x_\rho \gamma_\lambda}{v \cdot x} \right) Y_A(\omega, \xi) \right\} \gamma_5 \right]_{\beta\alpha}, \end{aligned} \quad (8.1)$$

where the path-ordered gauge factors on l.h.s. are omitted for brevity. For the three-particle B -meson DA's the model suggested in [30] is used:

$$\begin{aligned} \Psi_A(\omega, \xi) &= \Psi_V(\omega, \xi) = \frac{\lambda_E^2}{6\omega_0^4} \xi^2 e^{-(\omega+\xi)/\omega_0}, \quad X_A(\omega, \xi) = \frac{\lambda_E^2}{6\omega_0^4} \xi(2\omega - \xi) e^{-(\omega+\xi)/\omega_0}, \\ Y_A(\omega, \xi) &= -\frac{\lambda_E^2}{24\omega_0^4} \xi(7\omega_0 - 13\omega + 3\xi) e^{-(\omega+\xi)/\omega_0}. \end{aligned} \quad (8.2)$$

In this model the parameter ω_0 is equal to the inverse moment λ_B of the B meson two-particle DA ϕ_B^+ . For the latter we use the ansatz suggested in [31]:

$$\phi_B^+(\omega) = \frac{\omega}{\omega_0^2} e^{-\frac{\omega}{\omega_0}}, \quad \phi_B^-(\omega) = \frac{1}{\omega_0} e^{-\frac{\omega}{\omega_0}}. \quad (8.3)$$

Appendix C: Functions entering LCSR (4.4)

Here we collect the expressions for the coefficient functions $F_n^{(DA)}(q^2, \omega)$ entering the answer for the correlation function in (4.4) and used to derive the LCSR (4.7). Below the shorthand notation $\sigma = \omega/m_B$, $\bar{\sigma} = 1 - \sigma$ is introduced:

$$F_1^{(\Psi A)}(q^2, \omega) = -\frac{3Q_b}{m_b^2} (m_s - m_B \bar{\sigma}) \left(\frac{2m_b}{m_B} - 1 \right) - \frac{3Q_s}{\bar{\sigma}^2 m_B^2 - m_s^2} (2\sigma - 1) (m_s - m_B \bar{\sigma}),$$

$$F_1^{(\Psi V)}(q^2, \omega) = \frac{3Q_b}{m_b^2} (m_s + m_B \bar{\sigma}) \left(\frac{2m_b}{m_B} - 1 \right) + \frac{3Q_s}{\bar{\sigma}^2 m_B^2 - m_s^2} (2\sigma - 1) (m_s + m_B \bar{\sigma}),$$

$$\begin{aligned} F_1^{(XA)}(q^2, \omega) &= -\frac{Q_b}{m_b^2} \left[\left(2 + \frac{m_b}{m_B} \right) - \frac{m_s}{\bar{\sigma} m_B} \left(1 + \frac{2m_b}{m_B} \right) \right] \\ &- \frac{Q_s}{\bar{\sigma}^2 m_B^2 - m_s^2} \left(1 - \frac{m_s}{\bar{\sigma} m_B} \right) - \frac{3m_B^2 Q_s}{(\bar{\sigma}^2 m_B^2 - m_s^2)^2} (2\sigma - 1) \left(\frac{m_s^2}{m_B^2} - \bar{\sigma}^2 \right), \end{aligned}$$

$$F_1^{(YA)}(q^2, \omega) = -\frac{4Q_b}{m_b^2} \left(1 - \frac{m_b}{m_B}\right) - \frac{4Q_s}{\bar{\sigma}^2 m_B^2 - m_s^2} - \frac{6m_s m_B Q_s}{(\bar{\sigma}^2 m_B^2 - m_s^2)^2} (2\sigma - 1) \left(\frac{m_s}{m_B} - \bar{\sigma}\right),$$

$$F_2^{(\Psi A)}(q^2, \omega) = F_2^{(\Psi V)}(q^2, \omega) = 0,$$

$$F_2^{(XA)}(q^2, \omega) = -\frac{Q_b}{m_b^2} \left\{ \left(\bar{\sigma} m_B^2 - \frac{m_s^2}{\bar{\sigma}} \right) \left[\left(\frac{m_s}{m_B} + \bar{\sigma} \right) + \frac{2m_b}{m_B} \left(\frac{m_s}{m_B} - \bar{\sigma} \right) \right] \right. \\ \left. - q^2 \left[1 - \frac{2m_b}{\bar{\sigma} m_B} \left(\bar{\sigma} - \frac{m_s}{m_B} \right) + \frac{m_s}{m_B} \frac{4\sigma - 3}{\bar{\sigma}} \right] \right\} \\ + \frac{Q_s}{\bar{\sigma}^2 m_B^2 - m_s^2} \left(1 - \frac{m_s}{\bar{\sigma} m_B} \right) \left\{ q^2 (2\sigma - 1) + m_B^2 \left[\bar{\sigma}^2 (2\sigma + 1) + \frac{m_s}{m_B} \left(2\bar{\sigma} + (1 - 2\sigma) \frac{m_s}{m_B} \right) \right] \right\},$$

$$F_2^{(YA)}(q^2, \omega) = -\frac{2Q_b}{m_b^2} \left\{ 2q^2 \left(\bar{\sigma} - \frac{m_b}{m_B} \right) \right. \\ \left. + m_B (m_s - \bar{\sigma} m_B) \left[2\bar{\sigma} \left(1 - \frac{m_b}{m_B} \right) - \frac{m_s}{m_B} \left(1 - 4 \frac{m_b}{m_B} \right) \right] \right\} \\ + \frac{2Q_s}{\bar{\sigma}^2 m_B^2 - m_s^2} \left\{ m_B^2 \left(\bar{\sigma} - \frac{m_s}{m_B} \right) \left[2\bar{\sigma}^2 + \frac{m_s}{m_B} (4\sigma - 1) \right] - 2q^2 (1 - 2\sigma) \right\}. \quad (8.4)$$

Finally, we present the substitution relations for the integrals in (4.4):

$$\int_0^\infty d\omega \frac{f_1(q^2, \omega)}{(p - \omega v)^2 - m_s^2} \rightarrow - \int_0^{\omega_0} \frac{d\omega}{1 - \omega/m_B} f_1(q^2, \omega) e^{-s/M^2}, \\ \int_0^\infty d\omega \frac{f_2(q^2, \omega)}{[(p - \omega v)^2 - m_s^2]^2} \rightarrow \int_0^{\omega_0} \frac{d\omega}{(1 - \omega/m_B)^2} \frac{f_2(q^2, \omega)}{M^2} e^{-s/M^2} \\ + \frac{\eta(\omega_0)}{m_B} \frac{e^{-s_0/M^2}}{(1 - \omega_0/m_B)^2} f_2(q^2, \omega_0), \quad (8.5)$$

where $f_{1,2}$ is the product of the function $F_{1,2}^{(DA)}$ and the corresponding DA (the latter integrated over ξ), and

$$s = \omega m_B + \frac{m_s^2 - q^2 \omega / m_B}{1 - \omega / m_B}, \quad \eta(\omega_0) = \left[1 + \frac{m_s^2 - q^2}{(m_B - \omega_0)^2} \right]^{-1}, \\ \omega_0 = \frac{(s_0 + m_B^2 - q^2) - \sqrt{(s_0 + m_B^2 - q^2)^2 + 4m_B^2(m_s^2 - s_0)}}{2m_B}.$$

References

- [1] I. Bediaga *et al.* [LHCb Collaboration], arXiv:1208.3355 [hep-ex].
- [2] R. Aaij *et al.* [LHCb Collaboration], Phys. Rev. Lett. **108** (2012) 181806.

- [3] R. Aaij *et al.* [LHCb Collaboration], *JHEP* **1207** (2012) 133.
- [4] R. Aaij *et al.* [LHCb Collaboration], arXiv:1209.4284 [hep-ex].
- [5] J. -T. Wei *et al.* [BELLE Collaboration], *Phys. Rev. Lett.* **103** (2009) 171801.
- [6] J. P. Lees *et al.* [BABAR Collaboration], *Phys. Rev. D* **86** (2012) 032012.
- [7] T. Aaltonen *et al.* [CDF Collaboration], *Phys. Rev. Lett.* **107** (2011) 201802.
- [8] M. Beneke, Th. Feldmann and D. Seidel, *Nucl. Phys. B* **612** (2001) 25; *Eur. Phys. J. C* **41**, 173 (2005).
- [9] A. Khodjamirian, Th. Mannel, A. A. Pivovarov and Y.-M. Wang, *JHEP* **1009** (2010) 089.
- [10] C. Bobeth, G. Hiller and G. Piranishvili, *JHEP* **0712** (2007) 040.
- [11] M. Bartsch, M. Beylich, G. Buchalla and D. -N. Gao, *JHEP* **0911** (2009) 011.
- [12] B. Grinstein, M.J. Savage and M.B. Wise, *Nucl. Phys.* **B319** (1989) 271; M. Misiak, *Nucl. Phys.* **B393** (1993) 23; A.J. Buras and M. Munz, *Phys. Rev.* **D52** (1995) 186.
- [13] G. Buchalla, A. J. Buras and M. E. Lautenbacher, *Rev. Mod. Phys.* **68** (1996) 1125.
- [14] M. Beneke, G. Buchalla, M. Neubert and C. T. Sachrajda, *Phys. Rev. Lett.* **83** (1999) 1914; *Nucl. Phys. B* **606** (2001) 245.
- [15] H. H. Asatrian, H. M. Asatrian and D. Wyler, *Phys. Lett. B* **470** (1999) 223.
- [16] H. H. Asatrian, H. M. Asatrian, C. Greub and M. Walker, *Phys. Lett. B* **507** (2001) 162.
- [17] H. H. Asatryan, H. M. Asatrian, C. Greub and M. Walker, *Phys. Rev. D* **65** (2002) 074004.
- [18] M. Beneke and T. Feldmann, *Nucl. Phys. B* **592** (2001) 3.
- [19] F. De Fazio, T. Feldmann and T. Hurth, *Nucl. Phys. B* **733** (2006) 1 [Erratum-ibid. *B* **800** (2008) 405].
- [20] J. Beringer *et al.* [Particle Data Group Collaboration], *Phys. Rev. D* **86** (2012) 010001.
- [21] Y. Amhis *et al.* [Heavy Flavor Averaging Group Collaboration], arXiv:1207.1158 [hep-ex].
- [22] M. A. Shifman, A. I. Vainshtein and V. I. Zakharov, *Nucl. Phys. B* **147** (1979) 385, 448.
- [23] C. Bruch, A. Khodjamirian and J. H. Kuhn, *Eur. Phys. J. C* **39** (2005) 41.
- [24] T. Feldmann and J. Matias, *JHEP* **0301** (2003) 074.
- [25] R. Aaij *et al.* [LHCb Collaboration], *Phys. Rev. Lett.* **108** (2012) 231801.
- [26] A. Ali, P. Ball, L. T. Handoko and G. Hiller, *Phys. Rev. D* **61** (2000) 074024.
- [27] G. Buchalla and G. Isidori, *Nucl. Phys. B* **525** (1998) 333; B. Grinstein and D. Pirjol, *Phys. Rev. D* **70** (2004) 114005; C. Bobeth, G. Hiller and D. van Dyk, *JHEP* **1007** (2010) 098; M. Beylich, G. Buchalla and T. Feldmann, *Eur. Phys. J. C* **71** (2011) 1635.
- [28] J. Charles *et al.* [CKMfitter Group Collaboration], *Eur. Phys. J. C* **41** (2005) 1.
- [29] H. Kawamura, J. Kodaira, C. -F. Qiao and K. Tanaka, *Phys. Lett. B* **523** (2001) 111 [Erratum-ibid. *B* **536** (2002) 344].
- [30] A. Khodjamirian, T. Mannel and N. Offen, *Phys. Rev. D* **75** (2007) 054013.
- [31] A. G. Grozin and M. Neubert, *Phys. Rev. D* **55** (1997) 272.